

2012•2013
FACULTEIT GENEESKUNDE EN LEVENSWETENSCHAPPEN
*master in de biomedische wetenschappen: klinische
moleculaire wetenschappen*

Masterproef

Evaluation of iron oxide labeling as a tool for long term cell tracking and its effects on human dental pulp stem cell differentiation

Promotor :
dr. Tom STRUYS

Copromotor :
dr. Wendy MARTENS

De transnationale Universiteit Limburg is een uniek samenwerkingsverband van twee universiteiten in twee landen: de Universiteit Hasselt en Maastricht University.

Jessica Ratajczak

Masterproef voorgedragen tot het bekomen van de graad van master in de biomedische wetenschappen, afstudeerrichting klinische moleculaire wetenschappen



Universiteit Hasselt | Campus Hasselt | Martelarenlaan 42 | BE-3500 Hasselt
Universiteit Hasselt | Campus Diepenbeek | Agoralaan Gebouw D | BE-3590 Diepenbeek



Maastricht University

2012•2013

FACULTEIT GENEESKUNDE EN
LEVENSWETENSCHAPPEN

*master in de biomedische wetenschappen: klinische
moleculaire wetenschappen*

Masterproef

Evaluation of iron oxide labeling as a tool for long
term cell tracking and its effects on human dental pulp
stem cell differentiation

Promotor :
dr. Tom STRUYS

Copromotor :
dr. Wendy MARTENS

Jessica Ratajczak

*Masterproef voorgedragen tot het bekomen van de graad van master in de biomedische
wetenschappen, afstudeerrichting klinische moleculaire wetenschappen*

Table of contents

TABLE OF CONTENTS	I
PREFACE	III
LIST OF ABBREVIATIONS	V
ABSTRACT	VII
SAMENVATTING	IX
1 INTRODUCTION	1
1.1 HUMAN DENTAL PULP STEM CELLS	1
1.2 MAGNETIC RESONANCE IMAGING FOR STEM CELL TRACKING.....	3
1.2.1 <i>Basic principles of magnetic resonance imaging</i>	4
1.2.2 <i>Superparamagnetic iron oxide nanoparticles as labeling probes for magnetic resonance imaging</i> .	4
1.3 RESEARCH AIMS AND EXPERIMENTAL SETUP	6
2 MATERIALS & METHODS	9
2.1 SUBJECTS AND CELL CULTURE.....	9
2.2 LABELING HDPSCs WITH POLY-L-LYSIN (PLL) CONJUGATED ENDOREM®	9
2.3 DENTAL PULP STEM CELL DIFFERENTIATION.....	9
2.3.1 <i>Adipogenic differentiation of hDPSCs</i>	10
2.3.2 <i>Osteogenic differentiation of hDPSCs</i>	10
2.4 TRANSMISSION ELECTRON MICROSCOPY (TEM)	10
2.5 HISTOCHEMICAL STAININGS.....	11
2.6 IMMUNOCYTOCHEMISTRY	11
2.7 <i>IN VITRO</i> MAGNETIC RESONANCE IMAGING OF SPIO/POLY-L-LYSIN LABELED HDPSCS	12
2.8 RNA-ISOLATION, CDNA SYNTHESIS AND RT-PCR	12
2.9 SUBCUTANEOUS INJECTION OF SPIO-LABELED ADIPOGENIC INDUCED HDPSCS.....	14
2.10 <i>IN VIVO</i> MAGNETIC RESONANCE IMAGING OF ADIPOGENIC INDUCED HDPSCS.....	14
2.11 STATISTICAL ANALYSIS	14
3 RESULTS	15
3.1 MORPHOLOGICAL FEATURES OF HUMAN DENTAL PULP STEM CELLS	15
3.2 EXPLANT-DERIVED HDPSCs EXPRESS STEM CELL MARKERS CD105, CD146 AND STRO-1	15
3.3 SPIO LABELING OF HDPSCS RESULTS IN INTRACELLULAR ACCUMULATION OF IRON DEPOSITS	17
3.4 ADIPOGENIC DIFFERENTIATION POTENTIAL OF SPIO/PLL LABELED HDPSCS	18
3.4.1 <i>SPIO labeling does not interfere with the production of lipid droplets in adipogenic induced hDPSCs</i> 18	
3.4.2 <i>Adipogenic induced hDPSCs show de novo expression of lipoprotein lipase mRNA</i>	20
3.4.3 <i>T2* signal intensity is significantly decreased by 250 SPIO-labeled A-hDPSCs/μL</i>	22

Table of contents

3.4.4	250 labeled A-hDPSCs/ μ l significantly lower T2 relaxation time in vivo.....	23
3.5	OSTEOGENIC DIFFERENTIATION OF SPIO/PLL LABELED hDPSCS	24
3.5.1	Osteogenic differentiation of hDPSCs induces matrix production and substantial label dilution.....	24
3.5.2	Osteogenic induced hDPSCs produce extracellular matrix	25
3.5.3	Osteocalcin and Runt-related transcription factor-2 are expressed by hDPSCs and O-hDPSCs.....	25
3.5.4	Osteogenic differentiation leads to an upregulation of the protein osteocalcin	27
3.5.5	T2* signal intensity is significantly decreased by 500 SPIO-labeled O-hDPSCs/ μ L	28
3.5.6	Increasing SPIO concentrations leads to an increased accumulation of intracellular iron deposits....	28
4	DISCUSSION	31
5	CONCLUSION & SYNTHESIS	39
6	REFERENCES.....	41
	SUPPLEMENTAL INFORMATION	45
S1.	SUPPLEMENTAL MATERIALS & METHODS	45
S1.1	Neurogenic differentiation of hDPSCs	45
S2.	SUPPLEMENTAL DATA.....	45
S2.1	SPIO labeling does not interfere with neurosphere formation or cellular outgrowth	45

Preface

These last eight months I have been given the opportunity to perform my senior internship at the Department of Morphology at the University of Hasselt. Over these last few months I've experienced all the different aspects of scientific research. From the excitement of getting your first results, to the realization that things don't always go as planned and the curiosity that motivates every scientist to keep on exploring. Together, all these different facets made me realize that I made the right choice, when I started this journey five years ago. Therefore, I would like to take this opportunity to express my gratitude to all the people who joined me on this exciting (and sometimes frightening) rollercoaster ride!

First of all, I would like to thank Prof. dr. Ivo Lambrichts, for giving me the opportunity to do my internship with his research group. But most of all, I would like to thank him for making me feel part of the team, for taking time out of his busy schedule to discuss my research and for sharing his never ending stream of ideas and his remarkable insights.

A big thank you goes out to my promoters dr. Tom Struys and dr. Wendy Martens. Tom, thank for your support and guidance, but also for the trust you placed in me, allowing me to grow as an independent scientist. Wendy, thank you for your valuable criticism and all your help with my PCR experiments and especially thank you for your positive mindset and words of encouragement in times of need.

This projects would not have been possible without external help. Therefore, a word of appreciation for Prof. dr. Constantinus Politis from Ziekenhuis Maas en Kempen and Dr. Luc Vrielinck from the Ziekenhuis Oost-Limburg, for providing me with patient material. Furthermore, I would like to thank Prof. dr. Uwe Himmelreich and dr. Tom Dresselaers from the KUL department of Medical Imaging for their expertise on the MRI experiments.

A word of appreciation also goes out to Jeanine Santermans and Marc Jans. Thank you Jeanine for your advice on my immunostainings and for helping me with my (often challenging) quest for antibodies. Marc, thank you for meticulously preparing the samples for TEM analysis.

Furthermore, I would to thank Petra, Pascal and Kathleen. Petra, you were always ready to answer my questions and I very much enjoyed our scientific (and less scientific) conversations. I'll keep my fingers crossed for a sunny wedding day! Pascal, thank you for your help with the neurogenic differentiations and for sharing your (precious) growth factors. Kathleen, I appreciated the tips and tricks involving qPCR and thank you for helping me (struggle) with the analysis software. I really enjoyed working with all of you!

I would also like to thank my fellow students, Anuschka, Nazim, Manolo and Jasmine. Over these last eight months we've shared an "office", many coffee breaks, laughs and frustrations. Chloë, Esther and Sam, we all performed our internships at different locations, but I very much enjoyed hearing about your research, your funny lab stories and of course about the long list of Italian admirers. I always appreciated your advice and never ending encouragements and wish you all the best for the years to come!

Finally I would like to thank my family and friends for their continuous support and motivation throughout the years.

List of abbreviations

α -MEM	Minimal Essential Medium with alpha modification
A-hDPSCs	Adipogenic induced human dental pulp stem cells
bFGF	Basic fibroblastic growth factor
BM-MSCs	Bone marrow mesenchymal stem cells
DPSCs	Dental pulp stem cells
EGF	Epidermal growth factor
F	Fungizone
FABP-4	Fatty Acid Binding Protein-4
FCS	Fetal calf serum
FDA	Food and Drug Administration
FGF-8	Fibroblastic growth factor-8
hDPSCs	Human dental pulp stem cells
hMSC	Human mesenchymal stem cell
HSCs	Hematopoietic stem cells
LPL	Lipoprotein lipase
MRI	Magnetic resonance imaging
MSCs	Mesenchymal stem cells
MPIO	Micron-sized superparamagnetic iron oxide
NSCs	Neural stem cells
OCN	Osteocalcin
OD	Optical density
P	Penicillin
PBS	Phosphate buffered saline
PDL	Periodontal ligament
PFA	Paraformaldehyde
PLL	Poly-L-lysine
PPAR- γ	Peroxisome proliferator-activated receptor gamma
ROS	Reactive oxygen species
RT-PCR	Reverse Transcription Polymerase Chain Reaction
RunX2	Runt-related transcription factor-2
S	Streptomycin
SCAPs	Stem cells of the apical papilla
SCs	Stem cells
SHH	Sonic hedgehog
SPIO	Superparamagnetic iron oxide
TEM	Transmission electron microscope
USPIO	Ultrasmall superparamagnetic iron oxide

Abstract

Introduction: Human dental pulp stem cells (hDPSCs) are a subtype of mesenchymal stem cells which possess self-renewal capacity, high proliferation potential and the ability to undergo multi-lineage differentiation. Therefore, hDPSCs are considered plausible candidates for cell-based therapies. When considering cell therapy, non-invasive and non-toxic imaging techniques are necessary to evaluate and improve stem cell therapy. Magnetic labeling of the transplanted stem cells by means of superparamagnetic iron oxide (SPIO) nanoparticles, allows *in vivo* visualization using magnetic resonance imaging (MRI). In this study it is hypothesized that SPIO nanoparticles can be used for long-term *in vivo* monitoring of hDPSCs, without affecting their differentiation potential.

Materials & Methods: hDPSCs were isolated from human third molars and labeled with SPIO particles conjugated to poly-L-lysine prior to adipogenic and osteogenic differentiation. Differentiated cells were subjected to immunocytochemical analysis and RT-PCR experiments to investigate the expression of lineage specific markers. Furthermore, long-term label efficiency was evaluated based on histochemical stainings, TEM analysis and both *in vitro* and *in vivo* MRI.

Results: SPIO labeling (15 $\mu\text{g}/\text{mL}$) did not interfere with the adipogenic differentiation potential of hDPSCs as histochemical staining and TEM analysis showed the co-localization of lipid droplets and SPIO-containing endosomes. Furthermore, adipogenic differentiation of both labeled and unlabeled hDPSCs induced *de novo* expression of lipoprotein lipase (LPL). MRI, TEM and histochemical analysis also showed the presence of SPIO labels after adipogenic differentiation. *In vivo* MRI was performed to detect subcutaneously injected labeled adipogenic induced hDPSCs (A-hDPSCs). Transplants of labeled A-hDPSCs lead to a significant decrease in T2 relaxation compared to unlabeled control cells. Osteogenic differentiation of labeled hDPSCs induced matrix production and upregulation of osteocalcin protein expression. *In vitro* MRI yielded a significant decrease in T2* signal intensity, however, the increase in MRI contrast was barely detectable by eye. Therefore, SPIO concentration was increased to 25 and 50 $\mu\text{g}/\text{mL}$ in order to increase the detectability of the cells during visual interpretation of the MR-images. The highest concentration of SPIO particles resulted in the lowest fraction of unlabeled cells after osteogenic induction.

Discussion: This study demonstrated the ability of SPIO-labeled hDPSCs to undergo both adipogenic and osteogenic differentiation *in vitro*. Furthermore, results indicated that labeling conditions need to be optimized for different experiments, mainly depending on the expected degree of cellular proliferation. The ability to non-invasively track stem cell transplants will contribute immensely to the evaluation of cell-based therapies. Since cell-based therapies are currently being investigated as possible alternative treatment options in several clinically important domains (e.g. neurology and cardiology), optimization of SPIO-labeling could eventually contribute to the improvement of cell therapy in several major research areas

Samenvatting

Inleiding: Humane dentale pulpastamcellen (hDPSCs) behoren tot de groep van mesenchymale stamcellen. Deze cellen hebben multipotente eigenschappen, vertonen een hoog proliferatie gehalte en bezitten de capaciteit voor zelfvernieuwing. Daarom worden hDPSCs beschouwd als geschikte kandidaten voor stamceltherapieën. Niet-invasieve beeldvormingstechnieken zijn erg belangrijk voor de evaluatie en uiteindelijke verbetering van stamceltherapieën. Met behulp van superparamagnetische ijzeroxide (SPIO) labels kunnen getransplanteerde stamcellen *in vivo* worden opgevolgd door middel van magnetische resonantie beeldvorming (MRI). Deze studie veronderstelt dat SPIOs gebruikt kunnen worden om stamcellen op lange termijn op te volgen en dat deze partikels de differentiatie capaciteiten van de stamcellen niet beïnvloeden.

Materiaal & Methoden: hDPSCs werden geïsoleerd uit wijsheidstanden en gelabeld met SPIO partikels in combinatie met poly-L-lysine. Nadien werden de cellen adipogeen en osteogeen gedifferentieerd. De aanwezigheid van specifieke adipogene en osteogene merkers in de gedifferentieerde cellen werd geëvalueerd met behulp van immunocytochemie en RT-PCR. Verder werd het behoud van SPIO partikels na differentiatie onderzocht met behulp van transmissie elektronen microscopie (TEM) en MRI.

Resultaten: Het adipogeen differentiatie potentieel van de hDPSCs werd niet beïnvloed door de aanwezigheid van SPIOs (15 µg/mL) aangezien histochemische kleuringen, TEM en MRI analyse co-localisatie aantonen van vetdruppels en SPIO bevattende endosomen. Bovendien zorgde adipogene differentiatie ook voor de expressie van Lipoproteïne lipase (LPL). Zowel TEM als MRI resultaten geven duidelijk aan dat er voldoende labels aanwezig zijn na het doorlopen van het differentiatieproces om visualisatie mogelijk te maken. *In vivo* MRI beelden werden gebruikt om subcutaan getransplanteerde gelabelde adipogeen gedifferentieerde hDPSCs (A-hDPSCs) te lokaliseren. Transplanten van gelabelde A-hDPSCs waren in staat om de T2 relaxatietijd significant in te korten, in vergelijking met de niet gelabelde controle hDPSCs. Osteogeen gedifferentieerde hDPSCs produceerden matrix en vertoonden een toename in de expressie van osteocalcine. Het osteogeen differentieproces ging echter wel gepaard met een behoorlijke reductie van de labelinhoud, waardoor de gelabelde cellen moeilijk zichtbaar waren op T2* gewogen MRI beelden. Om de zichtbaarheid op T2* gewogen MRI beelden te verbeteren, werd de label concentratie verhoogd tot 25 en 50 µg/mL. De hoogste concentratie SPIOs resulteerde in de kleinste fractie van niet-gelabelde cellen, na het doorlopen van het differentiatieproces.

Discussie: Deze studie heeft aangetoond dat SPIO labeling het adipogeen en osteogeen differentiatie potentieel van hDPSCs niet beïnvloedt. De resultaten toonden echter wel aan dat de label condities voor ieder specifiek experiment geoptimaliseerd dienen te worden, afhankelijk van de verwachte celproliferatie. De mogelijkheid om de getransplanteerde stamcellen op een non-invasieve manier te kunnen opvolgen zal enorm bijdragen tot het verder ontwikkelen en het op punt stellen van stamceltherapieën. Aangezien stamceltherapie momenteel als een veel belovende behandelingsoptie wordt beschouwd voor een brede waaier van aandoeningen, zal deze labeling techniek uiteindelijk kunnen bijdragen aan veel verschillende onderzoeksgebieden

1 Introduction

Stem cell therapy is becoming a realistic alternative to conventional therapy and could potentially provide novel treatments options for patients with diseases for which there is currently little hope [1, 2]. Stem cells (SCs) are characterized as clonogenic cells with the capacity for self-renewal and multi-lineage differentiation [3]. Based on their developmental potential, SCs can be divided into three categories being totipotent, pluripotent and multipotent stem cells.

Although totipotent embryonic SCs can give rise to all cell types and this in sufficient numbers, their use is impeded due to ethical considerations, risk of malignant transformation and the possibility of immune rejection [4]. Therefore, (bio)medical research has shifted its interest towards the application of easily accessible and ethical less compromised SC sources . Adult organisms contain subpopulations of progenitor cells (termed adult SCs) that are responsible for tissue turnover and tissue regeneration in case of disease or injury [5]. Up to date, bone marrow is the most widely used source of adult SCs. Bone marrow contains two distinct stem cell populations being mesenchymal and hematopoietic stem cells (HSCs). HSCs are responsible for the replenishment of blood cells. Over the past years HSC transplantation has already been successfully applied to treat hematopoietic disorders in humans. However, their *in vitro* expansion is rather limited and they can evoke an immune response upon allogeneic transplantation [4].

The second population of SCs present in the adult bone marrow comprises the mesenchymal stem cells (MSCs). According to the International Society for Cellular Therapy MSCs are plastic adherent, express specific surface antigens and are able to differentiate towards osteogenic, adipogenic and chondrogenic lineages [6]. In contrast to HSCs, MSCs are considered suitable candidates for allogeneic transplantation since they do not express HLA class-II antigens or co-stimulatory molecules (CD40, CD80 and CD86) [7]. Moreover, MSCs have been described to produce growth factors and cytokines that might induce or facilitate repair of injured tissues [8]. Besides their immunomodulatory properties and their capacity for self-renewal, MSCs also show multi-lineage differentiation potential. Next to their mesodermal differentiation capacity (bone, cartilage and fat), they have also been shown to give rise to cardiomyocytes, hepatocytes and neural cells *in vitro* [4]. Therefore, adult MSCs have been suggested as suitable candidates for cell-based therapies.

1.1 Human dental pulp stem cells

Despite the extensive amount of research being performed with BM-MSCs, the possible therapeutic benefits of these SCs is partly offset by the invasiveness of the bone marrow isolation procedure and the associated donor site morbidity [9]. Although MSCs were firstly isolated from bone marrow, they

are also found in a variety of other easily accessible organs ranging from umbilical cord blood and placenta to adult adipose tissue and teeth [10-12].

Tooth development requires interactions between ectomesenchymal cells, originating from migrating neural crest cells and oral epithelial cells. The mutually inductive signaling leads to the formation of an outer layer of enamel and an inner layer of mineralized dentin (Figure 1). While the enamel is derived from the oral epithelium, dentin is synthesized by odontoblasts, which originate from the dental papilla. The dental papilla also gives rise to the soft fibrous pulp tissue that occupies the central chamber of teeth (Figure 1). The dental pulp is not only infiltrated by a network of blood vessels but also densely innervated. The periodontal ligament (PDL), which is derived from the dental follicle, is responsible for holding the tooth structure in place in the surrounding bone (Figure 1)[13].

Upon mechanical trauma or bacterial invasion resulting from caries, adult teeth are able to undergo limited reparative processes which can be categorized as reactionary (secondary) and reparative (tertiary) dentin formation. The latter involves the formation of reparative dentin by odontoblasts, which arise from precursor cells from the dental pulp [13]. The fact that severe tooth damage – which penetrates both enamel and dentine and into the pulp – stimulates repair processes, led to the idea that the tooth pulp might contain MSCs [14].

Recently, it has been demonstrated that different parts of the tooth contain stem cell populations. These include cells from the periodontal ligament that links the tooth root with the bone, cells from the tips of developing roots (apical pads), cells from the tissue surrounding the impacted tooth (dental follicle) and from the pulp of both exfoliated and adult teeth (Figure 1)[14].

In the adult teeth these dental pulp stem cells (DPSCs) are activated in response to mechanical trauma, exposure to chemicals or by disease processes. The repair processes include the formation of reparative dentin-like complexes composed of tubular mineralized matrix with odontoblasts and fibrous tissue containing blood vessels [12, 15]. Since Gronthos et al. demonstrated that DPSCs are able to produce reparative dentin both *in vitro* and *in vivo*, DPSCs were further characterized and compared to the extensively studied bone-marrow derived MSCs (BM-MSCs). Immunophenotypical analysis showed that DPSCs share a similar pattern of protein expression with BM-MSCs *in vitro* [16]. hDPSCs are adherent fibroblast-like cells, expressing commonly used mesenchymal stem cell markers such as CD29, CD44, CD105, CD146 and STRO-1. Given the appropriate growth conditions, hDPSCs have the ability to differentiate towards classical mesodermal lineages (adipogenic, chondrogenic and osteogenic lineages) [9, 12]. Compared to BM-MSCs, hDPSCs show a broader potency to differentiate towards neurogenic lineages, most likely due to their neural crest origin [16]. Furthermore, neuronally predifferentiated hDPSCs have been shown to express neuronal markers

and exhibit voltage dependent sodium and potassium channels but most importantly they have been shown to actively integrate into rat brain *in vivo* [17].

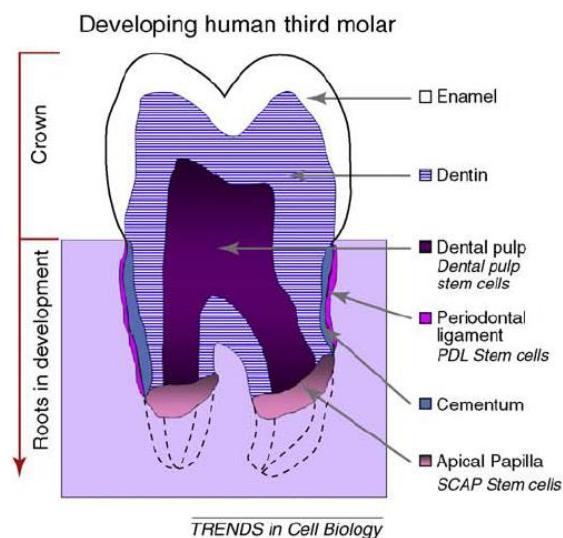


Figure 1. Diagram of a developing human third molar. A developing human third molar consisting of an outer layer of enamel, an inner layer of dentin and a central chamber occupied by pulp tissue. The developing third molar contains three subpopulations of dental SCs: dental pulp stem cells (DPSCs), periodontal ligament (PDL) stem cells and stem cells of the apical papilla (SCAP). Adapted from Volponi et al. 2010 [14].

Their ease of isolation and expansion, multi-lineage differentiation potential and immunomodulatory properties together with their potential for tissue regeneration, make hDPSCs promising candidates for future cell-based clinical applications. Possible applications of hDPSCs transplantations include tissue replacement, immunological modulation of the microenvironment and the promotion of tissue repair by the release of (neuro)trophic factors [18]. The capacity to home and engraft long-term into the target tissue is an important requirement for successful tissue replacement. MSCs have been shown to display a tropism for inflammatory and tumor micro-environments [19]. These particular micro-environments of injured tissues or tumors express specific receptors or chemokines to facilitate MSCs migration [20, 21]. Together, these facts illustrate the great therapeutic potential of MSC-based stem cell therapy. However, certain questions concerning the homing, engraftment and safety of the transplanted cells are yet to be answered [19].

1.2 Magnetic resonance imaging for stem cell tracking

When considering cell-based therapy, the longitudinal observation of cell transplants is an important question to be addressed in pre-clinical as well as clinical research. At present, the fate of transplanted cells is usually evaluated by means of histological analysis. Cells are tagged *in vitro* prior to transplantation for the purpose of histological analysis. Cells can be tagged via transfection with reporter genes, by using cyanine dyes or by selecting male donors and female recipients thereby using the Y chromosome as a marker [22]. Although histological analysis can provide detailed

information about the SCs after transplantation, it is unable to give spatio-temporal information and requires invasive isolation techniques [1]. Furthermore, due to the use of transgenic cells, these techniques are not suitable for clinical applications. In order to evaluate cell fate in a non-invasive and non-toxic manner, reliable cellular imaging techniques are necessary. Magnetic resonance imaging (MRI) is currently the most powerful diagnostic imaging tool for *in vivo* diagnosis and has been suggested as the most attractive imaging modality for *in vivo* stem cell tracking [23, 24].

1.2.1 Basic principles of magnetic resonance imaging

MRI is a non-invasive imaging tool with high spatial resolution. Conventional MR-images are based on the magnetic relaxation properties of hydrogen atoms. First an external magnetic field is applied to orient the dipoles with respect to the magnetic field. The orientation results in a net magnetization which is disturbed by radiofrequency pulses. The resulting magnetic relaxation profile can be used to produce a detailed image of the target tissue [25]. Depending on the incorporation of hydrogen atoms into the tissues, magnetic relaxation characteristics can differ. By manipulating the measurement settings, different relaxation profiles can be obtained. Depending on the measurement settings and the degree of structuring, tissues can have high or low signal intensities. In T1 weighted images – where T1 represents the spin-lattice relaxation time – structured hydrogen atoms appear as bright signals, while loosely bound hydrogen atoms have a low signal intensity. In the case of T2 weighted images – where T2 represents the spin-spin relaxation time – loosely bound hydrogen atoms show high signal intensities whereas hydrogen atoms in highly structured tissues show only low signal intensities [25, 26]. Finally, T2* relaxation is a combination of ‘true’ T2 relaxation and relaxation caused by magnetic field inhomogeneities. Magnetic susceptibility differences in tissues and materials lead to magnetic field inhomogeneities and thereby shorten T2* relaxations times, resulting in decreased signal intensity [27].

1.2.2 Superparamagnetic iron oxide nanoparticles as labeling probes for magnetic resonance imaging

Although MRI already provides excellent soft tissue contrast, the contrast can be further modulated either by using endogenous properties of the target tissue or by using exogenous contrast agents. The latter are commonly used to label cells *in vitro* prior to transplantation. When labeled with contrast agents, cell transplants can easily be distinguished from host cells by means of MRI-based cell imaging. Based on their mechanism of action, MR contrast agents can be divided into: (1) superparamagnetic materials, which create contrast by influencing the local magnetic field homogeneity, (2) paramagnetic compounds containing lanthanide chelates or Mn²⁺, which interfere with T1 and T2 relaxation times and finally (3) contrast agents that contain nuclei not present in the host such as ¹⁹F [28-30].

The most commonly used labeling approach uses superparamagnetic iron oxide (SPIO) nanoparticles as a contrast agent. SPIOs consist of ferric (Fe^{3+}) and ferrous (Fe^{2+}) ions. These particles disrupt the local magnetic field and produce magnetic susceptibility artifacts. By disrupting the local magnetic field, these magnetic moments decrease the T_2/T_2^* relaxation times. As a consequence, iron oxide based contrast agents appear as signal voids on T_2/T_2^* weighted MR-images [1]. Because of their large magnetic moments, the SPIO particles influence the magnetic field beyond their actual size, so even a small number of SPIO-loaded cells can be detected with *in vivo* MR-imaging.

Cellular labeling is achieved by adding SPIO nanoparticles to the growth medium during the *in vitro* cultivation period. The uptake of the particles is partially determined by the size of the particles. Based on their size, iron oxide based contrast agents can be classified as ultrasmall superparamagnetic iron oxide particles (USPIOs), SPIOs and micron-sized paramagnetic iron oxide particles (MPIOs). Larger particles such as the SPIOs and the MPIOs are more easily internalized than the USPIOs [31]. The uptake of these particles varies between cell types, but internalization can be improved by using transfection agents or by surface modification of the nanoparticles [32].

In order to increase stability and bio-compatibility, iron oxide particles are usually encapsulated by organic polymers. Dextran-coated SPIO particles such as Feridex[®] and Endorem[®] are already approved by the Food and Drug Administration (FDA) for hepatic imaging [33]. Although SPIOs are known to accumulate in Kupffer cells, they are not capable of efficiently labeling non-phagocytotic or slowly dividing cells *in vitro*. Label efficiency can be increased by combining SPIOs with DNA transfection agents such as Poly-L-lysine (PLL). The positive charge of PLL causes spontaneous but stable complex formation with the negatively charged SPIO particle. The complex formation is due to electrostatic interactions and initiates endocytosis of SPIO-PLL complexes, by altering the interactions between the SPIOs and the cell membrane [34]. Unfortunately, transfection agents have been described to interfere with differentiation of MSCs [35]. Furthermore, SPIO-PLL complexes have been shown to undergo endosomal degradation, resulting in high levels of reactive oxygen species (ROS) [36]. Endosomal degradation also results in cellular release of free iron, leading to unspecific MRI contrast [37]. Interfering with cell homeostasis may result in oncogenic cells, therefore it is of great importance to optimize SPIO labeling, for the safe and efficient labeling of SCs.

A recent study performed at our lab focused on optimizing the SPIO labeling protocol in order to maximize label efficiency and biocompatibility. In this study hDPSCs were labeled with dextran-coated SPIOs (Endorem[®]) conjugated to poly-L-lysine. This study achieved an *in vitro* detection limit of 50 labeled cells/ μL when hDPSCs were labeled with 15 $\mu\text{g}/\text{mL}$ SPIO particles in combination with 0.75 $\mu\text{g}/\text{mL}$ PLL. Based on tetrazolium salt assays these labeling conditions did not cause any adverse

effects on cell viability. Furthermore, Struys *et al.* transplanted labeled hDPSCs into the brain of immune-deficient mice for the purpose of *in vivo* MR-imaging. Animals were monitored for a period of two weeks and transplanted cells showed perfect label retention and no signs of tumorigenicity. These are promising data for future non-invasive monitoring of cell transplants in disease models and clinical studies [22]. Despite these promising results, it remains important to demonstrate efficient long-term labeling without detrimental effects on the differentiation capacity of hDPSCs [38].

1.3 Research aims and experimental setup

This study hypothesizes that iron oxide labeling can be used for long-term *in vivo* monitoring of hDPSCs, while preserving their differentiation potential. The aim of this study is twofold: firstly, to compare the osteogenic and adipogenic differentiation potential of SPIO-labeled and unlabeled hDPSCs; secondly, to demonstrate sufficient long-term labeling for *in vivo* monitoring of differentiated hDPSCs.

First of all, the MSC phenotype of the hDPSCs population is determined by the markers CD105, CD146 and STRO-1. Subsequently, magnetic labeling is achieved by adding SPIO-PLL mixtures (15 $\mu\text{g}/\text{mL}$ Endorem[®] + 0.75 $\mu\text{g}/\text{mL}$ PLL) to the culture medium. Poly-L-lysine is used as a transfection agent to facilitate the internalization of iron particles by the adherent hDPSCs. Once the labeling procedure is completed, adipogenic and osteogenic differentiation is induced. For adipogenic differentiation, cells are transferred to adipogenic differentiation medium containing hydrocortisone, isobutylmethylxanthine and indomethacin. Osteogenic differentiation medium contains dexamethasone, ascorbate phosphate and β -glycerol phosphate. Successful differentiation is assessed based on morphological and biochemical criteria. Adipogenic differentiation results in the presence of intracellular lipid droplets, which are visualized using an electron transmission microscope (TEM) or histochemically by means of Oil Red O staining. Furthermore, differentiated cells also express adipocyte-specific markers such as Fatty Acid Binding Protein-4 (FABP-4), which is demonstrated immunocytochemically. Osteogenic differentiation results in the production of cross-banded collagen and the occurrence of calcified matrix, which is visualized with TEM. Furthermore, osteogenic-induced hDPSCs also express osteogenic markers such as osteocalcin, which is demonstrated immunocytochemically. Furthermore, this study also includes a pilot experiment, investigating the effect of SPIO/PLL labeling on the neurogenic differentiation capacity of hDPSCs. Neurogenic induction is performed in two phases: (i) the induction phase, comprising neurosphere formation and (ii) the maturation phase, for neurosphere attachment and cellular outgrowth (*supplementary data*).

Secondly, this study aims to demonstrate sufficient long-term label retention for the *in vivo* monitoring of hDPSCs. Before starting *in vivo* experiments, label retention in differentiated hDPSCs is

evaluated by means of TEM, Perls' iron staining and by *in vitro* MR-imaging. Using a 9.4T Biospec small animal MR system, T2-maps and 3D high-resolution T2*-weighted images are taken for the evaluation of cell labeling after a culturing period of 3 weeks.

This study will provide more insight into the effects of iron oxide labeling on the adipogenic and osteogenic differentiation potential of hDPSCs. In addition, this study investigates the possibility to track SPIO-labeled cells, even after extended *in vitro* culturing periods. Every novel labeling method requires the demonstration of efficient long-term labeling without detrimental effects on cell phenotype and differentiation capacity, in order for successful implementation in clinical settings.

2 Materials & Methods

2.1 Subjects and cell culture

Healthy human third molars, extracted for therapeutic or orthodontic reasons were used, with the patient's informed consent. Teeth were fractured mechanically and pulp tissue was removed and collected in Minimal Essential Medium with alpha modification (α -MEM) supplemented with 10% heat-inactivated fetal calf serum (FCS; Biochrom AG, Berlin, Germany), 2mM L-Glutamin, 1% penicillin (P), 1% streptomycin (S). This particular medium composition will from now on be referred to as normal culture medium. Tissue was transferred to the laboratory for cell isolation. Tissues were washed with normal culture medium to remove contaminating blood cells and minced into fragments of 1-3 mm³. The explants were transferred to 6-well plates containing normal culture medium and were left undisturbed for 14 days to allow migration of cells from the explants. Cells were incubated at 37°C in a humidified atmosphere containing 5% CO₂ and medium was changed twice a week. After 14-21 days, explants were discarded and the resulting cell population was subcultured. During the cultivation process the explants and cell cultures were evaluated using a Nikon Eclipse TS100 inverted phase-contrast microscope equipped with a Jenoptik Progress C3 camera (Jenoptik, Jena, Germany) with corresponding Progress Capture Pro 2.7 software. All products were purchased from GIBCO Invitrogen Corp, Paisly, Scotland, United Kingdom unless stated otherwise.

2.2 Labeling hDPSCs with poly-L-lysine (PLL) conjugated Endorem®

The seeding density of hDPSCs prior to labeling with Endorem® (Guerbet, France) and poly-L-lysine (PLL; Sigma-Aldrich) is dependent on the experiment. Endorem® was conjugated with poly-L-lysine in order to facilitate the uptake of the SPIO particles. The 11.2 mg/mL Endorem® stock solution was diluted to a 5 mg/mL working solution, while the 0.2 mg/mL PLL stock solution was diluted to a 30 µg/mL working solution. To obtain SPIO-PLL mixtures the working solutions were diluted even further in α -MEM to obtain final concentrations of 15, 25 or 50 µg/mL Endorem® and 0.75 µg/mL PLL and placed on a rotating shaker for 60 minutes at room temperature. Afterwards, 0.1% FCS was added to the medium and hDPSCs cultures were incubated with an equal volume of SPIO-PLL complexes. After a 24 hours incubation (37°C) period, cells were washed three times and kept in normal culture medium for at least another 24 hours.

2.3 Dental pulp stem cell differentiation

In order to investigate the influence of SPIO particles on the differentiation potential of hDPSCs, these cells were subjected to adipogenic and osteogenic differentiation by incubating them in differentiation media from the hMSC Functional Identification Kit (R&D systems, UK).

2.3.1 Adipogenic differentiation of hDPSCs

Following trypsinization, hDPSCs were seeded either onto 12-mm \emptyset glass coverslips for light microscopy or onto plastic coverslips (Thermanox[®], Electron Microscopy Sciences, Hatfield, PA, United States of America) for electron microscopy at a density of 2.1×10^4 cells/cm². Cells were kept in normal culture medium and cultured at 37°C in a humidified atmosphere containing 5% CO₂. When 90-100% of confluence was reached, medium was changed to adipogenic induction medium (StemXVivo[™]; R&D Systems, UK; CCM011) containing hydrocortisone, isobutylmethylxanthine and indomethacin. Medium was changed twice a week and after 3 weeks, cells seeded on glass coverslips were washed with phosphate buffered saline (PBS) and fixed with 4% paraformaldehyde (PFA; Unifix, Duiven, The Netherlands) for 20 min at room temperature. Cells seeded on plastic coverslips were fixed with 2% glutaraldehyde in 0.05M cacodylate buffer (pH 7.3) overnight at 4°C.

2.3.2 Osteogenic differentiation of hDPSCs

Following trypsinization, hDPSCs were seeded either onto 12-mm \emptyset glass coverslips for light microscopy or onto plastic coverslips (Thermanox[®], Electron Microscopy Sciences) for electron microscopy at a density of 4.2×10^3 cells/cm². Cells were kept in normal culture medium at 37°C in a humidified atmosphere containing 5% CO₂. When 50-70% of confluence was reached, medium was changed to osteogenic differentiation medium (StemXVivo[™]; R&D Systems, UK; CM008) containing dexamethasone, ascorbatphosphate and β -glycerolphosphate. Medium was changed twice a week. After 3 weeks, cells seeded on glass coverslips were washed with PBS and fixed with 4% PFA (Unifix, Duiven, The Netherlands) for 20 min at room temperature. Cells seeded on plastic coverslips were fixed with 2% glutaraldehyde in 0.05M cacodylate buffer (pH 7.3) overnight at 4°C.

2.4 Transmission electron microscopy (TEM)

Cells seeded on plastic Thermanox[®] coverslips were fixed with 2% glutaraldehyde (Laborimpex, Brussels, Belgium) in 0,05M sodium cacodylate buffer (Aurion, Wageningen, The Netherlands) (pH=7,3) at 4°C. Afterwards, the samples were washed with 0,05M sodium cacodylate (pH=7,3) and 0,15M saccharose at 4°C. Postfixation was performed by incubating the samples with 2% osmiumtetroxide (Aurion, Wageningen, The Netherlands) in 0,05M sodium cacodylate buffer (pH=7,3) for 1 hour at 4°C. Subsequently, the cell seeded coverslips were dehydrated by putting them through a dehydrating series of graded concentrations of acetone. The dehydrated samples were then impregnated overnight in a 1:1 mixture of acetone and araldite epoxy resin (Aurion, Wageningen, The Netherlands) at room temperature. After impregnation, samples were embedded in araldite epoxy resin at 60°C using the pop-off method and cut into slices of 40-60nm, using a Leica EM UC6 microtome (Leica, Groot Bijgaarden, Belgium). Slices were mounted on 50 mesh copper grids (Aurion, Wageningen, The Netherlands) coated with 0,7% formvar. TEM analysis was performed

using a Philips EM208 S electron microscope (Philips, Eindhoven, The Netherlands). Digital images were captured with a Morada Soft Imaging System camera and processed with ITEM-FEI software (Olympus SIS, Münster, Germany).

2.5 Histochemical stainings

SPIO particles were visualized using Perls' iron staining. Cells were stained for 40 minutes with a 1:1 mixture of 2% potassium hexacyanoferrate (II) trihydrate ($3[\text{Fe}(\text{CN})_6]^{4-}$; Vel n.v., Heverlee, Belgium) and 2% hydrochloric acid (HCl; Vel n.v). Trivalent iron particles (Fe^{3+}) form blue precipitates referred to as Prussian Blue. After washing with distilled water, nuclei were counterstained using Mayer's haematoxylin and cells were mounted with aqueous mounting medium (Aquatex; Merck, Darmstadt, Germany).

Adipogenic differentiation of hDPSCs was evaluated by means of different histological staining techniques. Adipogenic differentiation was determined using 0.3% Oil Red O to demonstrate the presence of lipid droplets in the cell cytoplasm. Stained cells were visualized using a photomicroscope equipped with an automated digital camera (Nikon Eclipse 80i).

2.6 Immunocytochemistry

To evaluate the expression of mesenchymal, adipogenic and osteogenic markers, hDPSCs were seeded onto glass coverslips. The expression of mesenchymal markers (CD105, CD146, STRO-1), the osteogenic marker OCN and adipogenic marker FABP-4 was evaluated by means of immunofluorescence. When confluent, cells were fixed with 4% PFA for 20 min at room temperature. Next, cells were permeabilized with 0.05% Triton-X for 30 min at 4°C and non-specific binding sites were blocked with 10% normal donkey serum for 20 min at room temperature. Cells were incubated overnight with primary antibodies (Table 1). After washing with PBS, cells were incubated with either donkey anti-mouse, anti-rabbit or anti-goat secondary antibodies, which were either conjugated to an Alexa 555 or an Alexa 488 fluorophore (Invitrogen). Cells were counterstained using DAPI (Sigma) and mounted in Fluorescent Mounting Medium (Dako). The immunoreactivity was evaluated using a Nikon Eclipse 80i microscope (Nikon, Kingston, UK) and analyzed with NIS elements BR 4.0 software (Nikon). To quantify the expression of adipogenic and osteogenic markers, the mean fluorescent intensity was measured ($n=10$) for different culture conditions using NIS elements BR 4.0 Software.

Table 1: Primary antibodies for immunocytochemistry

Antibody	Host	Dilution	Supplier
<i>Phenotyping</i>			
CD 105	mouse	1/250	Millipore
CD 146	rabbit	1/100	Abcam
STRO-1	mouse	1/50	R&D systems
<i>Adipogenic markers</i>			
FABP-4	goat	1/10	R&D systems
<i>Osteogenic markers</i>			
OCN	mouse	1/100	Abcam

FABP-4 = Fatty Acid Binding Protein-4; OCN = osteocalcin

2.7 *In vitro* magnetic resonance imaging of SPIO/poly-L-lysine labeled hDPSCs

For MRI-based evaluation of cellular labeling, labeled hDPSCs were pelleted at 300g and resuspended in PBS. Using a 1:1 ratio of 250 μ l PBS and 250 μ l 0.5% agar in distilled water, cell suspensions of 1, 5, 10, 25, 50, 250 and 500 cells/ μ l were transferred to 0.5mL eppendorfs, 1/3 prefilled with solidified agar. After hardening of the cell mixtures, eppendorfs were filled completely with 0.5% agar and placed in a purpose-built Teflon holder and transferred to a plastic cup. The Teflon holder was completely immersed in agar and capped. Phantoms were imaged using an 9.4 Tesla Biospec experimental animal MRI scanner (BioSpec, Bruker BioSpin, Ettlingen, Germany) equipped with an actively shielded gradient set of 600 mT m⁻¹. A 7.2 cm quadrature resonator (Bruker BioSpin, Ettlingen) was used for radio-frequency irradiation and detection. After acquisition of localizer images, T₂ maps were acquired using a multi-slice-multi-echo protocol (MSME, spin echo sequence) with the following parameters: TR=3000 ms and 16 TE increments of 10 ms, 256² matrix, field-of-view 5.5 x 5.5 cm, 6 slices of 0.35 cm thickness. High-resolution 3D T₂*- weighted MR-images were acquired using a gradient echo sequence (FLASH, TR=200 ms, TE=15 ms, flip angle 27°). The field-of-view was 5.5 x 5.5 x 1.6 cm and the isotropic resolution was 125 μ m. Images were processed and analyzed with Paravision 5.0 (Bruker BioSpin, Ettlingen, Germany).

2.8 RNA-isolation, cDNA synthesis and RT-PCR

Total RNA was isolated using the RNeasy Plus Minikit (Qiagen, Venlo, The Netherlands) according to manufacturer's instructions. RNA concentration and purity was evaluated by measuring the optical density at 260nm and the 260/280nm ratio using a NanoDrop spectrophotometer (Isogen Life Science, IJsselstein, The Netherlands).

Total RNA was reverse transcribed into cDNA using the Reverse Transcription System (Promega, Leuven, Belgium). Briefly, RNA was supplemented with 25 mM MgCl₂, 10x RTase buffer, 10mM dNTP mixture; 20-40 U/μl RNasin; 20U/μl AMV RTase; 500μg/mL Oligo(dt) primer and nuclease free water. The reverse transcription reaction was performed on 42°C for 60 minutes, 95°C for 5 minutes, using the iCYCLER (Biorad Benchmark).

Table 2: Composition of PCR mastermix and applied PCR protocol

PCR mix per sample (μL)		PCR program			
10x PCR buffer	2,5	Denaturation	1x	5'	94°C
10mM dNTP mix	0,5	Denaturation	35x	1'	95°C
25μM Forward-Primer	1	Annealing		1'	55/60°C
25μM Reverse-Primer	1	Elongation		45''	72°C
1U/μL Taq polymerase	0,75	Elongation	1x	10'	72°C
MiliQ	18,25		1x	∞	4°C
cDNA	1				

RT-PCR reactions were performed by means of Taq DNA polymerase (1 U/μL; Roche Diagnostics, Vilvoorde, Belgium) according to the protocol in Table 2. PCR reactions were performed using a BioRad Thermal cycler under following conditions: a denaturation step (94°C, 5min) followed by amplification over 35 cycles of subsequent denaturation (95°C, 1min); annealing (temperature dependent on primers, 1min) and elongation (72°C, 45sec). The reaction was completed by a final elongation step (72°C, 10min). All primers were purchased from Eurogentec S.A. (Seraing, Belgium) and are listed in Table 3. Afterwards, PCR products were separated on a 1.2% agarose gel (Invitrogen) together with a 100 bp ladder (Invitrogen).

Table 3: Primer sequences for Reverse Transcription Polymerase Chain Reaction (RT-PCR).

Gene	Sequence (5'-3')	Bases	Product size (bp)	T _m (°C)
<i>Runx2</i>	Fw: CAG-ACC-AGC-AGC-ACT-CCA-TA	20	176	62
	Rev: CAG-CGT-CAA-CAC-CAT-CAT-TC	20		60
<i>OCN</i>	Fw: AGC-AAA-GGT-GCA-GCC-TTT-GT	20	63	60
	Rev: GCG-CCT-GGG-TCT-CTT-CAC-T	19		62
<i>PPAR-γ</i>	Fw: CAG-TGG-GGA-TGC-TCA-TAA	18	422	54
	Rev: CTT-TTG-GCA-TAC-TCT-GTG-AT	20		56
<i>LPL</i>	Fw: AGT-GGC-CAA-ATA-GCA-CAT-CC	20	186	60
	Rev: CCG-AAA-GAT-CCA-GAA-TTC-CA	20		58
<i>ActB</i>	Fw: GAT-CAT-TGC-TCC-TCC-TGA-GC	20	228	58
	Rev: AAA-GCC-ATG-CCA-ATC-TCA-TC	20		56

RunX2 = Runt-Related transcription factor-2; OCN = Osteocalcin; PPAR_γ = Peroxisome proliferator-activated receptor gamma; LPL = Lipoprotein lipase; ActB = β-actin.

2.9 Subcutaneous injection of SPIO-labeled adipogenic induced hDPSCs

hDPSCs were labeled with 15 µg/mL SPIO and 0.75 µg/mL PLL prior to adipogenic induction. After three weeks, adipogenic differentiated hDPSCs (A-hDPSCs) were trypsinized and resuspended at a concentration of 250 cells/µL in 250 µL of growth factor-reduced Matrigel (BD Biosciences, Erembodegem, Belgium). For control samples, 250 unlabeled hDPSCs/µL were dissolved in 250 µL growth factor-reduced Matrigel. All experimental protocols were approved by the Ethical Committee of Hasselt University and in accordance with international standards on animal welfare. Four male C57BL/6 mice (Harlan CPB, Zeist, The Netherlands) were subcutaneously injected with 250 µL of growth factor-reduced Matrigel containing either unlabeled hDPSCs or SPIO-labeled A-hDPSCs. Injections were performed under isofluran-induced anesthesia (1-2%; Iso-Vet; Eurovet, Bladel, The Netherlands)

2.10 *In vivo* magnetic resonance imaging of adipogenic induced hDPSCs

MRI was performed 24 hours after injection of the Matrigel using a Bruker Biospec 9.4 Tesla small animal MR scanner (Bruker BioSpin, Ettlingen, Germany; horizontal bore, 20 cm) equipped with actively shielded gradient insert (1200 mT/m) and a 3.5 cm quadrature coil (Bruker Biospin, GE). For localization purposes respiration triggered 3D RARE (TR 1000ms, TE 8.1ms rarefactor 16, resolution 22µm isotropic) and 3D FISP (TR 6ms TE 1.4ms scan repetition time 1500ms, resolution 200µm isotropic) sequences were used . T2 values were determined using a MSME sequence (TR 4s TE:10-100ms, 15slices of 0.8mm thick, resolution200µm in plane). T2* was determined using a multiple gradient echo sequence (TR=4s, TE=1.6ms, 8 echo's at 1.ms inter-echo delay, same geometry as for MSME). Data were processed using the scanners software (Paravision 5.1).

2.11 Statistical analysis

Statistical analysis was performed with GraphPad Prism 5.01 software (GraphPad software Incorporated, La Jolla, USA). Depending on the dataset, significant differences between experimental groups were determined with one way analysis of variance (ANOVA) and Tukeys, Dunnett's or Bonferroni's multiple comparison post-hoc test. Differences between two experimental groups were determined using a paired Student t-Test after checking for Gaussian distribution with D'Agostino and Pearson omnibus normality test. Results are presented as means ± standard error of mean (SEM). A significant difference was stated when the p-value was smaller than 0.05. (* p-value < 0.05, ** p-value < 0.01, *** p-value < 0.001).

3 Results

3.1 Morphological features of human dental pulp stem cells

Dental pulp tissue was isolated from human third molars and mechanically minced into fragments of 1-3mm³. These fragments were brought into culture to allow outgrowth of hDPSCs using the explant culture technique. The pulp explants attached to the plastic culture dishes and after one week in culture, outgrowth of adherent hDPSCs was observed (Figure 2A). The resulting hDPSCs population is a heterogeneous population comprising spindle shaped (arrow) cells as well as polygonal (arrowhead) cells (Figure 2B).

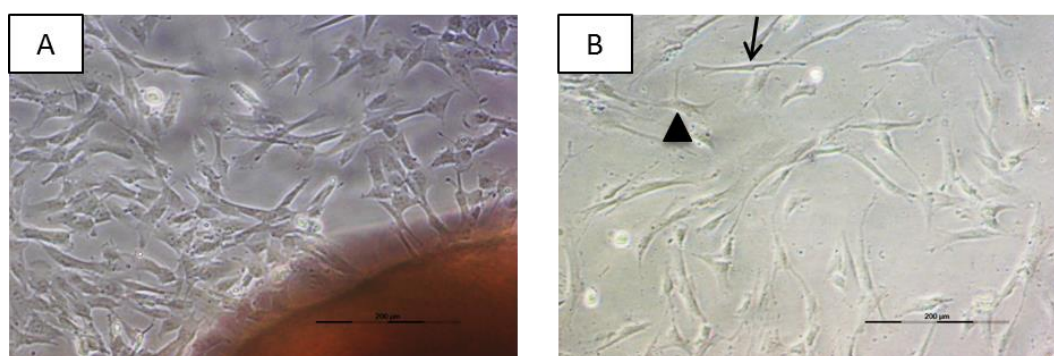


Figure 2: Morphological features of hDPSCs (B) when cultured via the explant methodology (A). hDPSCs are isolated using the explant methodology (A). Cells migrate out of tissue explants and confluency is reached after 10-14 days. Cultured hDPSCs are plastic adherent and display a mesenchymal-like cell morphology comprising both spindle shaped (arrow) and polygonal (arrowhead) cell types (B). hDPSCs = human dental pulp stem cells (Scale bar = 200µm)

3.2 Explant-derived hDPSCs express stem cell markers CD105, CD146 and STRO-1

Immunocytochemical analysis was performed to verify the MSC phenotype of the hDPSCs populations used in this study. Surface antigens characteristic for MSCs include CD105, CD146 and STRO-1 (Figure 3). hDPSCs are positive for CD105 and display a granular staining pattern of the cell cytoplasm as well as the nucleus (Figure 3A-B). hDPSCs also show immunoreactivity for CD146. However, some inter-patient variability could be seen, resulting in subsets of stronger CD146⁺ cells in some cultures (Figure 3E). Furthermore, hDPSCs were found to express the suggested marker for more potent MSCs, STRO-1 (Figure 3G-H). Negative controls do not show non-specific binding sites for the secondary antibody (Figure 3C,F,I).

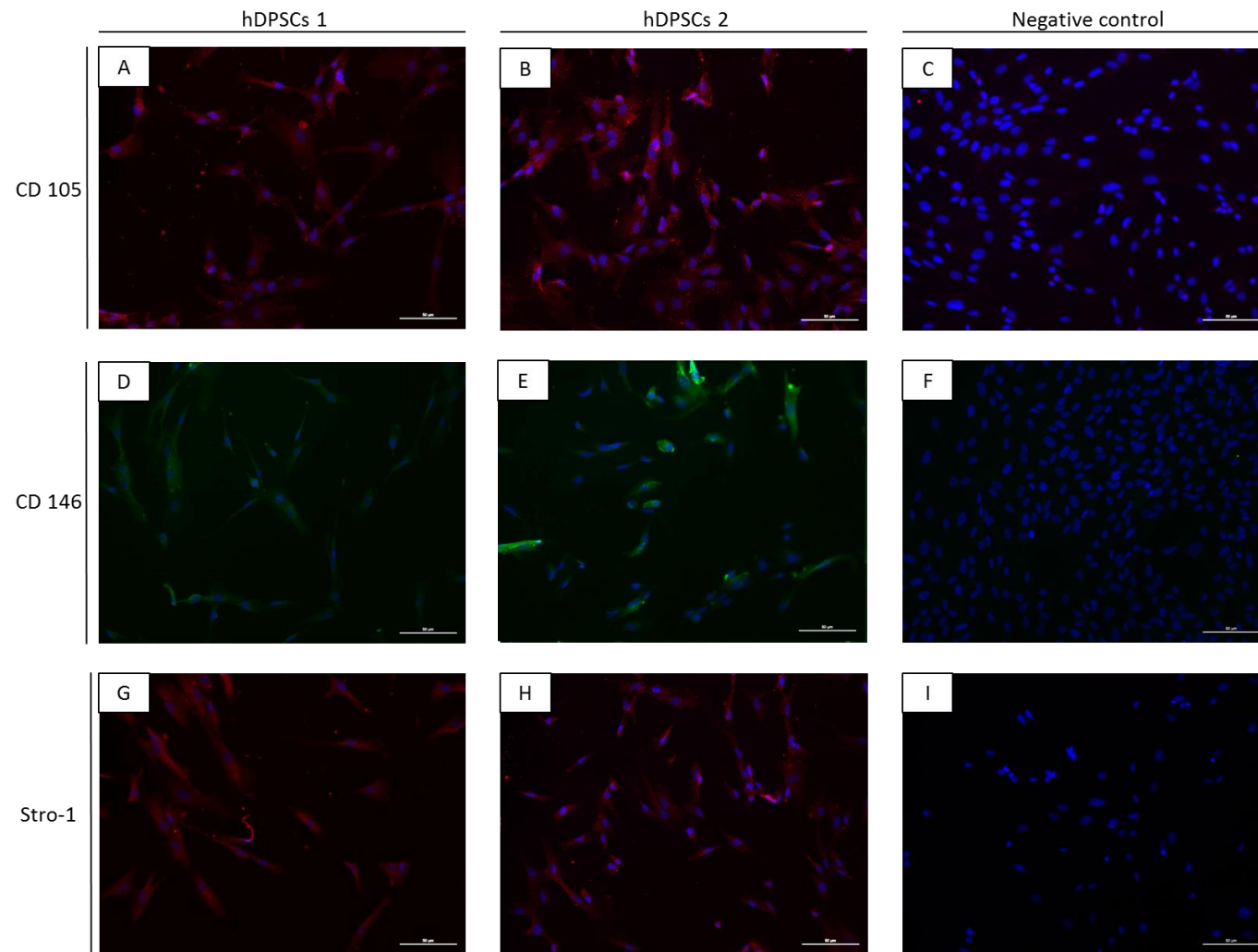


Figure 3: Explant-derived hDPSCs express stem cell markers CD105, CD146 and STRO-1. hDPSCs display a uniform expression pattern of CD105. (A-B) and show immunoreactivity for CD146 (D-E). The suggested marker for more potent MSCs, STRO-1 is found to be expressed in both stem cell populations (G-H). Negative controls do not show non-specific binding of the secondary antibody (C,F,I). hDPSCs = human dental pulp stem cells (Scale bar = 50μm)

3.3 SPIO labeling of hDPSCs results in intracellular accumulation of iron deposits

In order to investigate the influence of SPIO/PLL labeling on the differentiation potential of hDPSCs, cells were labeled prior to cell differentiation. Phase-contrast images of hDPSCs incubated for 24 hours with 15 $\mu\text{g}/\text{mL}$ SPIO conjugated to 0.75 $\mu\text{g}/\text{mL}$ poly-L-lysine showed no aberrant cell morphologies (Figure 4A). Gold-colored deposits represent the SPIO particles (black arrows) still residing within the cells after 24 hours of label-free culture (Figure 4A). SPIO uptake was also confirmed with Perls' iron staining combined with Mayer's haematoxylin for nuclear counterstaining. Perls' staining visualizes iron deposits (black arrows) as blue precipitates, revealing numerous intracellular iron deposits mainly residing in the peri-nuclear area. (Figure 4B).

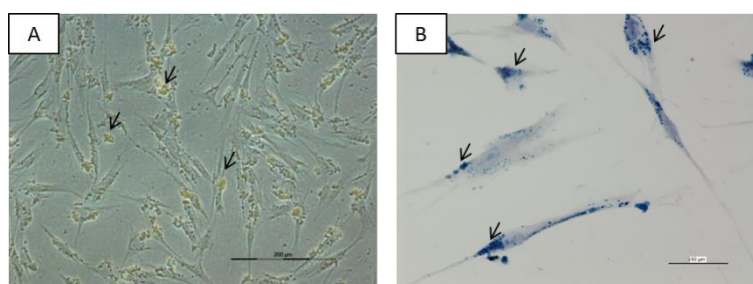


Figure 4: Intracellular iron deposits are present in hDPSCs after 24 hours of SPIO labeling. Phase-contrast images of SPIO/PLL labeled hDPSC show no aberrations in morphology and confirm cellular uptake of SPIO particles (**A**; black arrows). Perls' iron staining shows internalization of SPIO particles as blue precipitates (**B**; black arrows). hDPSCs = human dental pulp stem cells; PLL = poly-L-lysine; SPIO = superparamagnetic iron oxide (Scale bar A=200 μm ; B=50 μm)

Transmission electron microscopic (TEM) analysis was performed to further evaluate the location of SPIO particles and their influence on cell morphology (Figure 5). Ultrastructural analysis of hDPSCs labeled with 15 $\mu\text{g}/\text{mL}$ SPIO and 0.75 $\mu\text{g}/\text{mL}$ poly-L-lysine for 24 hours, shows SPIO-containing endosomes accumulating underneath the plasma membrane and residing in the peri-nuclear region (Figure 5A). Within the endosomes, the SPIO particles are homogeneously distributed and do not show signs of clustering (Figure 5B-C).

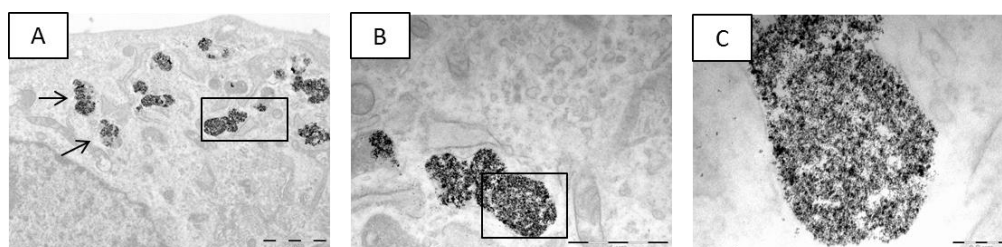


Figure 5: SPIO particles are homogeneously distributed within endosomes. Loading cells with SPIO particles results in the accumulation of SPIO-containing endosomes (black arrows) underneath the plasma membrane and residing in the peri-nuclear region (**A**). Panel (**B**) is an enlarged image of the boxed area in panel (**A**) and panel (**C**) is the enlarged image of the boxed area in panel (**B**). Within the endosomes, the SPIO particles show a homogeneous distribution, without any signs of particle clustering (**C**). SPIO = superparamagnetic iron oxide (Scale bare A= 2 μm ; B= 1 μm and C=0.2 μm)

3.4 Adipogenic differentiation potential of SPIO/PLL labeled hDPSCs

The adipogenic differentiation potential of labeled and unlabeled hDPSCs was tested by performing differentiation experiments with adipogenic-inducing medium (StemXVivo™, R&D systems) containing hydrocortisone, isobutylmethylxanthine and indomethacin. In this section, the adipogenic differentiation of SPIO/PLL labeled hDPSCs (A-hDPSCs) is evaluated based on morphological and ultrastructural criteria and compared to unlabeled hDPSCs. Furthermore, the production of lipid droplets as well as the expression of adipocyte related genes and proteins such as lipoprotein lipase (*LPL*) and Peroxisome proliferator-activated receptor gamma (*PPAR-γ*) and Fatty Acid Binding Protein-4 (*FABP-4*) is assessed. The efficiency of SPIO/PLL labeling for long-term *in vitro* cultures is investigated by means of MR-imaging (MRI). The possibility of tracking labeled A-hDPSCs *in vivo* is evaluated using MRI.

3.4.1 SPIO labeling does not interfere with the production of lipid droplets in adipogenic induced hDPSCs

In order to evaluate adipogenic differentiation, both labeled and unlabeled A-hDPSCs were stained with Oil red O, to reveal the presence of intracellular lipid droplets (Figure 6; arrows). Lipid droplets are located in the periphery of the cells with a more cuboidal morphology (Figure 6). In labeled A-hDPSCs the SPIO particles appear as gold-colored deposits after Oil red O staining (Figure 6B; arrow heads). In undifferentiated hDPSCs, no signs of lipid accumulation could be observed (Figure 6C).

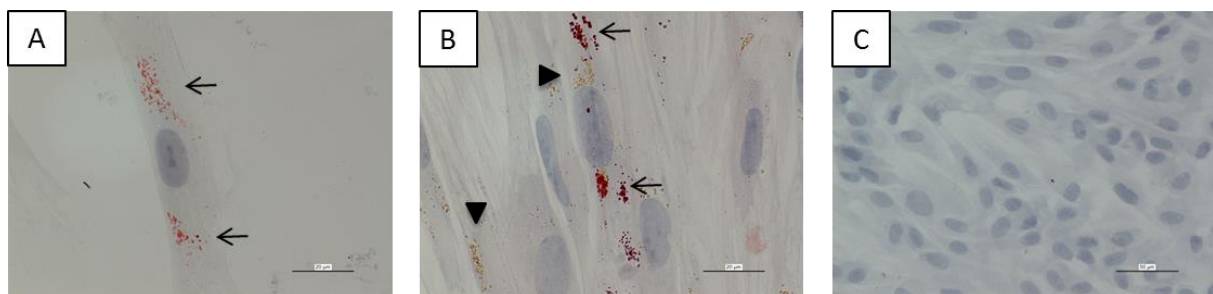


Figure 6: Both labeled and unlabeled hDPSCs contain lipid droplets after adipogenic induction. Successful adipogenic induction is confirmed by histochemical staining of lipid droplets with Oil red O. Lipid droplets (arrows) can be visualized in unlabeled (A) and SPIO-labeled (B) A-hDPSCs. SPIO-particles are visualized as gold-colored particles (arrowheads). hDPSCs = human dental pulp stem cells; SPIO = superparamagnetic iron oxide (Scale bar A,B = 20µm; C = 50µm)

Immunostaining with anti-Fatty Acid Binding Protein-4 (*FABP-4*) was performed to confirm adipogenic differentiation of hDPSCs. *FABP-4* positive cells (white arrows) were present in cultures of labeled and unlabeled A-hDPSCs. Furthermore, the increased *FABP-4* expression also coincided with the acquisition of a cuboidal morphology, characteristic for adipocytes (Figure 7B,C). In control cultures of undifferentiated hDPSCs containing SPIO particles, no cells were detected with an above baseline *FABP-4* expression level (Figure 7A). Despite the presence of *FABP-4* positive cells,

quantification did not yield a significant difference between differentiated and undifferentiated cultures (Figure 7D).

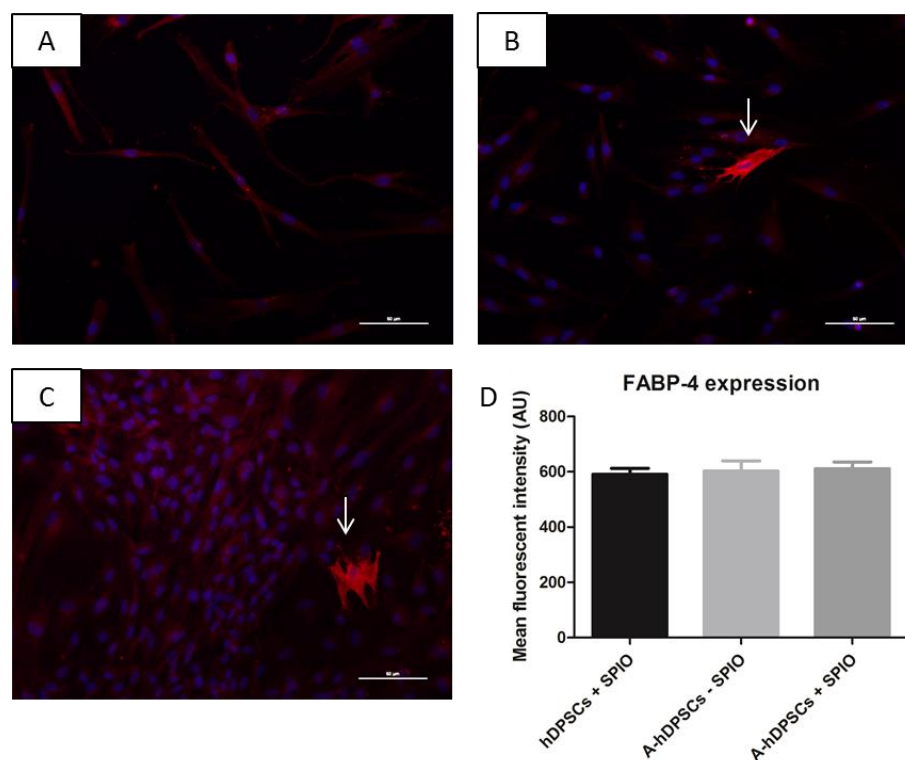


Figure 7: Adipogenic induction of hDPSCs results in FABP-4 positive cells. FABP-4 positive cells are detected in cultures of unlabeled (B) and labeled (C) hDPSCs, after three weeks of adipogenic differentiation. No clearly positive cells were detected in undifferentiated SPIO-labeled hDPSCs (A). Quantification of mean fluorescent intensity did not reveal any significant changes in FABP-4 expression between the different samples (D). Data were analyzed with One Way ANOVA and Tukeys multiple comparison post-test. Data are represented as S.E.M. A-hDPSC = adipogenic-induced human dental pulp stem cells; AU = arbitrary units; FABP-4 = Fatty Acid Binding Protein-4; SPIO = superparamagnetic iron oxide. (scale bar = 50 μ m)

After three weeks of adipogenic differentiation, SPIO labels are present in A-hDPSCs as demonstrated by the blue precipitates formed by Perls' iron staining (Figure 8, black arrows). Adipogenic differentiation resulted in the retraction of cellular processes and in a more cuboidal cell morphology (Figure 8; arrow head). Furthermore, adipogenic differentiation was found to be successful in labeled A-hDPSCs as evidenced by the co-localization of SPIO-particles (black arrows) and lipid droplets (Figure 6B; Figure 8; dotted arrows).

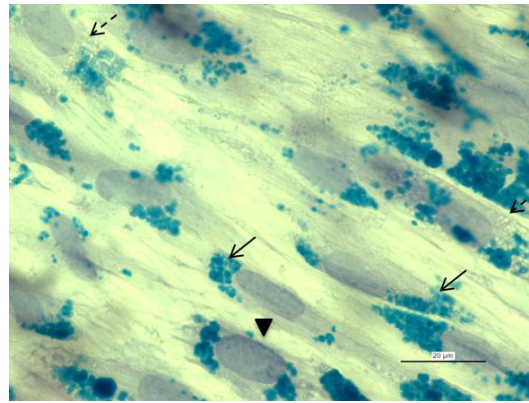


Figure 8: hDPSCs contain SPIO particles after adipogenic differentiation. Adipogenic differentiation of hDPSCs leads to a more cuboidal morphology (arrow head). Perl's iron staining visualizes SPIO particles as blue precipitates (black arrows). Furthermore, labeled cells also contain lipid droplets (dotted arrow). Cell nuclei were counterstained with Mayer's hematoxylin. hDPSCs = human dental pulp stem cells; SPIO = superparamagnetic iron oxide (Scale bar = 20 μ m)

Ultrastructural analysis of A-hDPSCs confirmed an altered cellular morphology as well as the co-localization of SPIO particles and lipid droplets (Figure 9). Adipogenic differentiation resulted in cells with a more cuboidal appearance (Figure 9A). TEM analysis revealed the intracellular accumulation of lipid droplets (Figure 9B, arrow heads) and confirmed the presence of SPIO particles (Figure 9B, arrow).

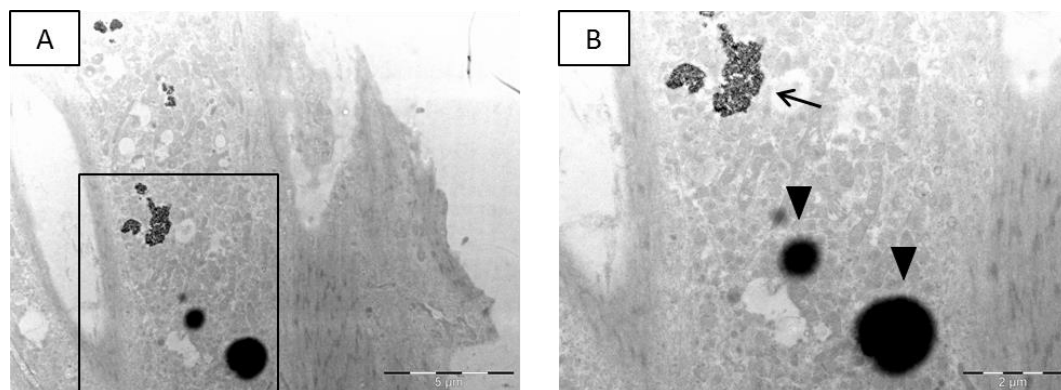


Figure 9: Ultrastructural analysis of adipogenic differentiated hDPSCs showing co-localization of lipid droplets and SPIO-containing endosomes. A-hDPSCs show a more cuboidal cell morphology (A). Panel (B) represents an enlargement of the boxed area in panel (A). Adipogenic differentiation results in the intracellular accumulation of electron-dense lipid droplets (B; arrow heads). After three weeks of *in vitro* culture, SPIO-containing endosomes (black arrow) can be detected in the cytoplasm (B). A-hDPSCs = adipogenic induced human dental pulp stem cells; SPIO = superparamagnetic iron oxide (Scale bar A=5 μ m; B=2 μ m)

3.4.2 Adipogenic induced hDPSCs show *de novo* expression of lipoprotein lipase mRNA

In order to evaluate the expression of adipocyte specific genes at mRNA level, RT-PCR was performed on cDNA samples of labeled (n=2) and unlabeled (n=1) A-hDPSCs as well as on undifferentiated (n=2) hDPSCs samples. After 3 weeks of adipogenic differentiation, *de novo* expression of the adipocyte-

specific transcript lipoprotein lipase (*LPL*; 186bp) was detected by RT-PCR (Figure 10). Neither undifferentiated control samples (Figure 10 1C; 2C) nor undifferentiated SPIO-labeled hDPSCs samples showed *LPL* expression (Figure 10 1S,2S). However, *LPL* expression was detected in samples of unlabeled A-hDPSCs (n=1) as well as in labeled A-hDPSCs (Figure 10 1A⁻, 1A⁺, 2A⁺). Housekeeping gene β -actin (*ActB*; 228bp) displays a decreased expression in control and labeled samples of one patient (Figure 10 1C, 1S), while it is uniformly expressed in all other samples.

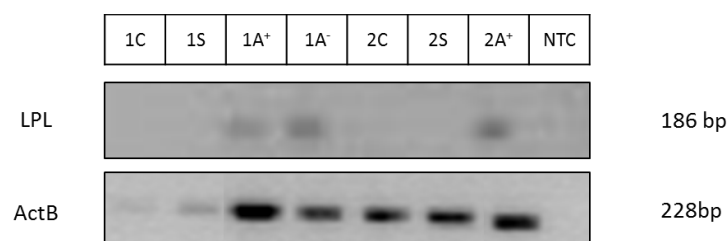


Figure 10: RT-PCR indicates *de novo* expression of lipoprotein lipase in labeled and unlabeled A-hDPSCs. All samples were loaded onto a 1.2% agarose gel. Undifferentiated hDPSCs with (1S, 2S) or without SPIO labeling (1C,2C) do not express *LPL* (186bp). Adipogenic induction causes *de novo* expression of *LPL* in both labeled A-hDPSCs (1A⁺, 2A⁺) and unlabeled A-hDPSCs (1A⁻). Except for 1C and 1S, β -actin (*ActB*, 228bp) shows a uniform expression pattern. A-hDPSCs = adipogenic-induced human dental pulp stem cells; *LPL* = lipoprotein lipase, *ActB* = β -actin, NTC= no template control.

Besides the expression of *LPL*, the expression of *PPAR- γ* (*PPAR- γ* , 422bp), another marker for adipogenic differentiation, was also evaluated by means of RT-PCR (Figure 11). In contrast to *LPL*, control samples and labeled samples also express *PPAR- γ* at mRNA level (Figure 11A-B; 1C,2C,1S,1S). For the purpose of a semi-quantitative evaluation of *PPAR- γ* expression, cDNA samples were diluted (1:1, 1:2, 1:5 and 1:10) and the intensities of the resulting bands were analyzed and normalized to the housekeeping gene β -actin (*ActB*; 228bp). Analysis of band intensities showed higher intensities for A-hDPSCs especially in undiluted cDNA samples (Figure 11B,D). Although the difference between differentiated and undifferentiated hDPSCs seems to diminish with increasing dilutions, band intensities for A-hDPSCs are always higher compared to control samples, except for one sample (Figure 11B; 1A⁻).

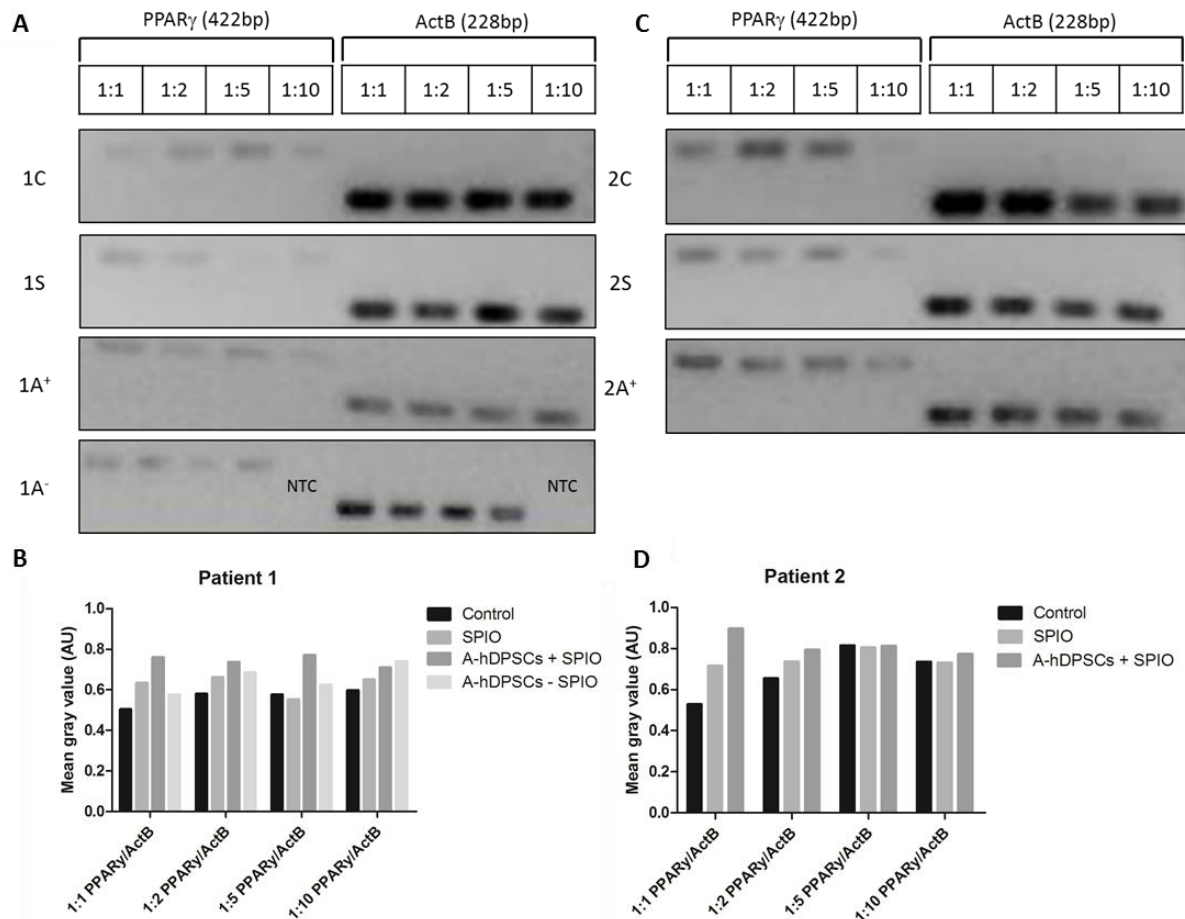


Figure 11. *PPAR- γ* is detected in both differentiated and undifferentiated hDPSCs. All samples were loaded onto a 1.2% agarose gel. *PPAR- γ* (422bp) was detected in all samples (A,C). However, after normalizing band intensities to *ActB* (228bp), the expression of *PPAR- γ* is found to be more pronounced in differentiated (1A⁺, 1A⁻, 2A⁺) samples compared to the undifferentiated (1C, 1S, 2C, 2S) samples (B,D). *ActB* = β -actin; A-hDPSCs = adipogenic induced human dental pulp stem cells; AU = arbitrary units; NTC = no template control; *PPAR- γ* = Peroxisome proliferator-activated receptor gamma; SPIO = superparamagnetic iron oxide

3.4.3 *T2** signal intensity is significantly decreased by 250 SPIO-labeled A-hDPSCs/ μ L

Phantoms ($n=2$) containing SPIO/PLL labeled A-hDPSCs were scanned using MR-imaging modality. The relative signal intensities on *T2**-weighted images were compared between different loading conditions after three weeks of *in vitro* culture (Figure 12). The relative signal intensities of *T2**-weighted MR-images were calculated and data were normalized by defining the control condition of one labeled cell/ μ L as 100% relative signal intensity (Figure 12B). An increase in MRI contrast can be observed by eye, starting from a concentration of 25 labeled cells/ μ L (Figure 12A; D-G). Increasing the concentration to 250 labeled cells/ μ L results in a significantly ($p<0.001$) decreased *T2** signal intensity (Figure 12B). Further increasing the amount of labeled cells to 500 cells/ μ L did not result in a more pronounced decrease in *T2** signal intensity ($p<0.001$; Figure 12B).

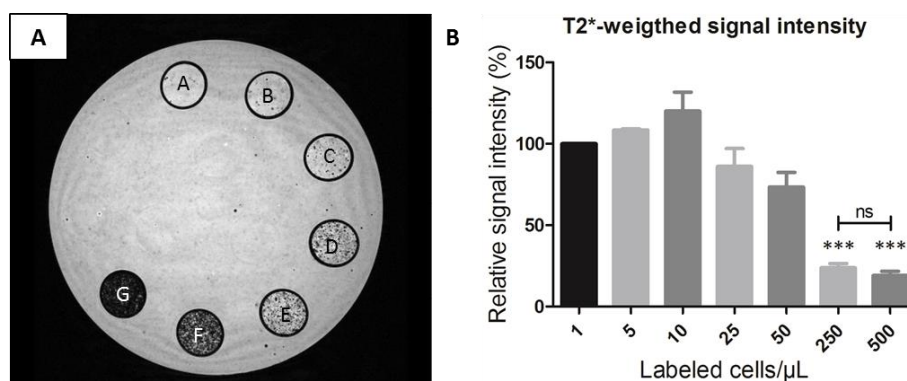


Figure 12: T2* signal intensity is significantly decreased by 250 SPIO-labeled A-hDPSCs/μL. A high resolution 3D T2*-weighted MRI-scan of A-hDPSCs, three weeks after labeling with 15μg/mL SPIO and 0.75μg/mL PLL, shows a gradual increase in MRI contrast, with increasing amounts of labeled A-hDPSCs (A). Analysis of relative T2* signal intensities indicates a decreasing trend in T2* signal intensity starting at a concentration of 25 labeled A-hDPSCs/μL (B). Increasing the number of labeled cells/μL to 250 significantly ($p < 0.001$) decreases T2* signal intensity. Doubling this concentration did not lead to a more pronounced decrease in T2* signal intensity ($p < 0.001$). Data were analyzed with one way ANOVA and Dunnett's and Bonferroni's multiple comparison post-test. Data are represented as S.E.M.; *** = p -value ≤ 0.001 . (A-B-C-D-E-F-G-H = respectively 1, 5, 10, 25, 50, 250 and 500 labeled cell(s)/μL). A-hDPSCs = adipogenic induced human dental pulp stem cells; MRI= magnetic resonance imaging; ns = not significant; PLL = poly-L-lysine; SPIO = superparamagnetic iron oxide.

3.4.4 250 labeled A-hDPSCs/μL significantly lower T2 relaxation time *in vivo*

Based on the results of the MRI phantoms, 250 labeled cells/μL were considered the optimal labeling condition and were used for *in vivo* experiments. C57BL/6 mice ($n=4$) were injected with Matrigel containing unlabeled hDPSCs (white arrow) on the left and labeled A-hDPSCs on the right (dotter arrow). Subcutaneous injection of 250 labeled A-hDPSCs/μL resulted in a complete decrease of T2* relaxation time, due to an inhomogeneous distribution of the cells within the Matrigel (Figure 13A). The complete signal quenching also leads to loss of anatomical information of the surrounding tissues on T2*-weighted MR-images. Therefore, T2 relaxation times were calculated from T2 maps (Figure 13B). Results show a significant ($p < 0.001$) decrease in T2 relaxation in the presence of 250 labeled A-hDPSCs/μL compared to unlabeled control conditions (Figure 13C). Furthermore, despite the inhomogeneous cellular distribution, T2 relaxation was not completely diminished and no anatomical information was lost due to SPIO-induced contrast changes (Figure 13B).

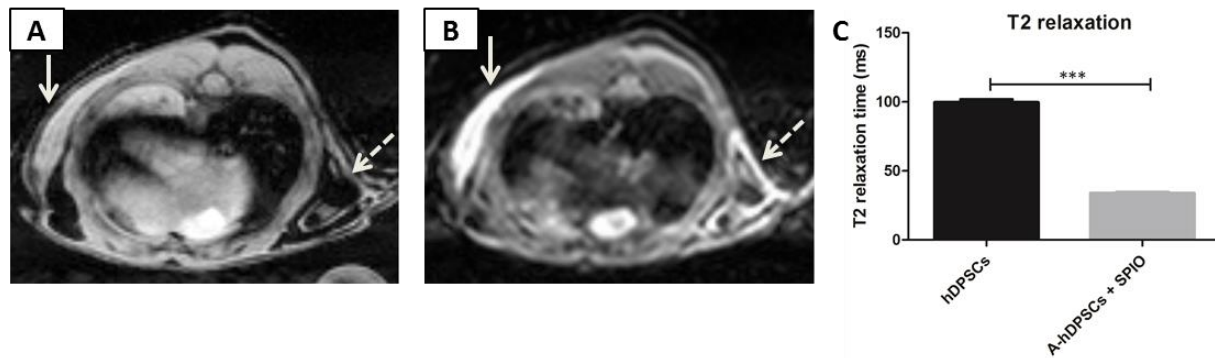


Figure 13: 250 labeled A-hDPSCs/ μ L significantly decrease T2 relaxation time *in vivo*. T2*-weighted MR-images showing the control Matrigel (white arrow) containing unlabeled hDPSCs on the left and labeled A-hDPSCs (dotted white arrow) on the right (**A**). Labeled A-hDPSCs were not homogenously distributed within the Matrigel leading to areas with T2* relaxation times of zero. Therefore, differences in contrast between unlabeled and labeled A-hDPSCs were evaluated based on T2-weighted MR-images (**B,C**). T2-weighted MR-images showing the control Matrigel (white arrow) containing unlabeled hDPSCs on the left and labeled A-hDPSCs (dotted white arrow) on the right (**B**). Analysis of T2 relaxation times showed a significant ($p < 0.001$) decrease in T2 relaxation in the presence of 250 labeled A-hDPSCs/ μ L ($n=4$) (**C**). Data were analyzed with a paired Student t-Test after checking for Gaussian distribution with D'Agostino and Pearson omnibus normality test. Data are represented as S.E.M.; *** = p -value ≤ 0.001 . A-hDPSCS = adipogenic induced human dental pulp stem cells; MR = magnetic resonance; SPIO = superparamagnetic iron oxide

3.5 Osteogenic differentiation of SPIO/PLL labeled hDPSCs

The influence of SPIO/PLL labeling on the osteogenic differentiation potential of hDPSCs was tested by subjecting both labeled and unlabeled hDPSCs to three weeks of osteogenic induction. In this section, the osteogenic differentiation of SPIO/PLL labeled hDPSCs is evaluated based on morphological and ultrastructural criteria and compared to osteogenic induced hDPSCs (O-hDPSCs) not subjected to SPIO labeling. Furthermore, the production of extracellular matrix and the expression of specific osteoblast related genes and proteins such as osteocalcin (*OCN*) and Runt-related transcription factor-2 (*RunX2*) is assessed. Finally, the efficiency of SPIO/PLL labeling for long-term *in vitro* cultures is determined based on MR-imaging.

3.5.1 Osteogenic differentiation of hDPSCs induces matrix production and substantial label dilution

Three weeks of osteogenic induction of labeled hDPSCs with dexamethasone, ascorbatphosphate and β -glycerolphosphate resulted in a polygonal cell morphology and multi-layered cell culture (Figure 14A). Osteogenic differentiation induced the production of small round calcified nodules, which can be visualized with a phase-contrast microscope (Figure 14A; arrow heads). After three weeks of *in vitro* culture, SPIO particles were detected with Perls' iron staining (Figure 14B; arrows). However, the label content is markedly decreased since the start of the differentiation process (Figure 4; Figure 14B).

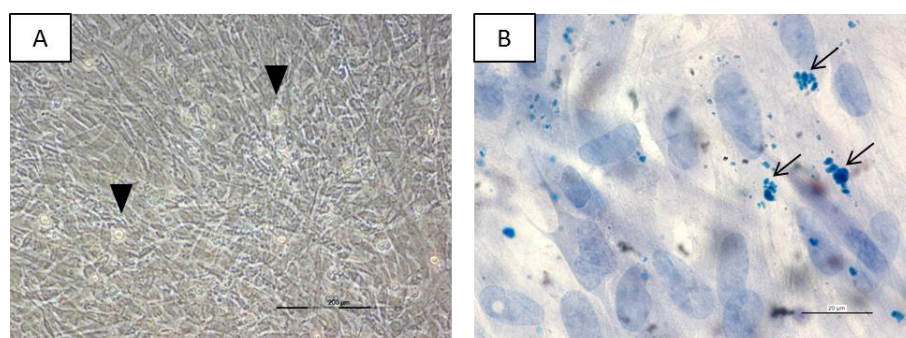


Figure 14: Osteogenic differentiation of hDPSCs induces matrix production and substantial label dilution. Visualization of osteogenic induced hDPSCs with a phase-contrast microscope demonstrated the presence of small round calcified nodules (**A**; arrow heads). Perl's iron staining showed the presence of a limited amount of SPIO labels in O-hDPSCs (**B**, arrows). O-hDPSCs = osteogenic induced human dental pulp stem cells; SPIO = superparamagnetic iron oxide (Scale bar A= 200μm; B = 20μm)

3.5.2 Osteogenic induced hDPSCs produce extracellular matrix

Ultrastructural analysis of O-hDPSCs confirmed the presence of SPIO particles (Figure 15B; arrow heads) after 3 weeks of *in vitro* culture. TEM analysis demonstrated the presence of extracellular matrix, mainly consisting of cross-banded collagen fibers (Figure 15A; dotted arrow), thereby further confirming the acquisition of an osteoblastic phenotype. The presence of mineralized matrix was also confirmed on the ultrastructural level (Figure 15B: black arrow).

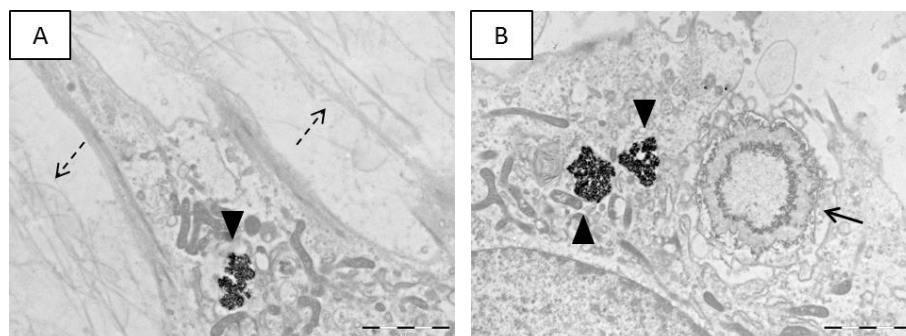


Figure 15: Osteogenic induced hDPSCs produce extracellular matrix. Osteogenic differentiation resulted in the production of extracellular matrix, mainly consisting of cross-banded collagen fibrils (**A**; dotted arrow). SPIO-containing endosomes were detected after three weeks of *in vitro* culture (arrow heads). The presence of round calcified nodules (**B**, black arrow) confirmed the osteoblastic phenotype. hDPSCs = human dental pulp stem cells; SPIO = superparamagnetic iron oxide (Scale bar = 2μm).

3.5.3 Osteocalcin and Runt-related transcription factor-2 are expressed by hDPSCs and O-hDPSCs

Osteogenic differentiation was evaluated based on the expression of osteoblast-specific genes at mRNA level by means of RT-PCR. Results demonstrate that the osteocalcin transcript (*OCN*, 63bp) is not only present in O-hDPSCs but also in labeled and unlabeled control samples (Figure 16A). Although *OCN* is expressed in all samples, expression levels vary between samples. After analysis of band intensities and normalization to the expression of β -actin (*ActB*, 228bp), some cultures (20,

2O⁺) showed increased *OCN* expression (Figure 16B). Some control samples (1C, 1S) yielded higher values after normalization due to the low expression of *ActB* in these samples. Analysis of band intensities did not reveal any apparent differences between *OCN* expression levels between labeled and unlabeled control conditions (Figure 16B)

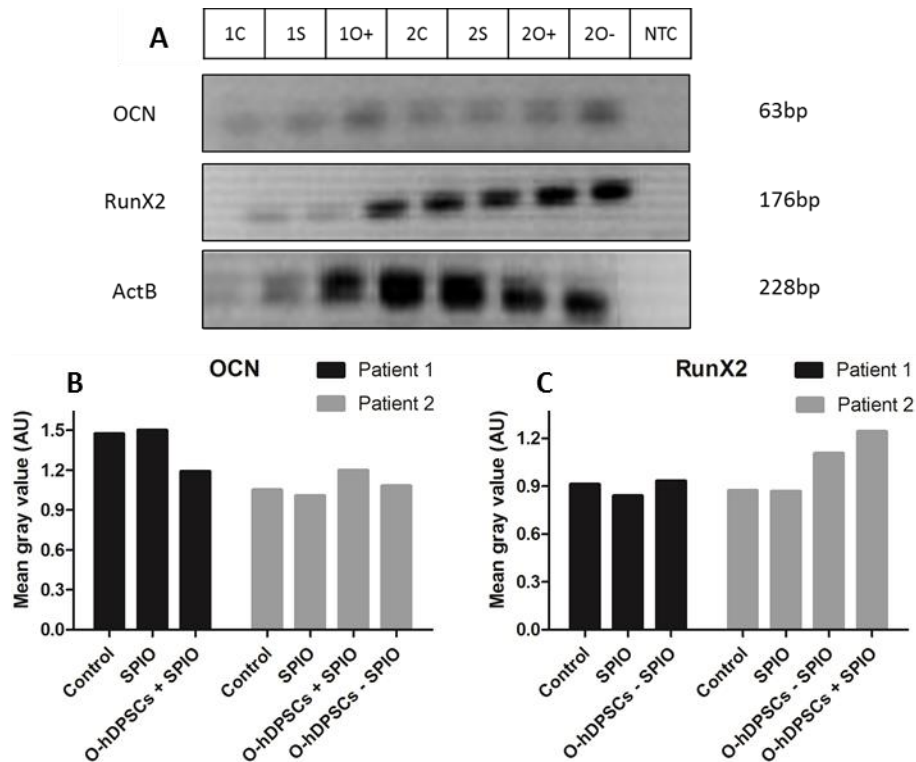


Figure 16: Expression of *OCN* and *RunX2* is slightly increased in labeled and unlabeled O-hDPSCs. All samples were loaded onto a 1.2% agarose gel. *OCN* (63bp) and *RunX2* (176bp) are present in all samples (A). Analysis of band intensities and normalization to *ActB* (228bp) reveals a minor increase in *OCN* expression in both labeled (1O⁺, 2O⁺) and unlabeled O-hDPSCs (2O⁻) (B). Some control samples (1C, 1S) yield higher values after normalization due to the low expression of *ActB* in these samples (B). Despite the clear difference in band intensity of *RunX2* control samples (1C,1S) and O-hDPSCs (1O⁺), only a minor difference could be demonstrated after normalization. Some samples (2O⁻, 2O⁺) showed a more pronounced increase in *RunX2* expression than others (1O⁺) (C). *ActB* = β -actin; *OCN* = osteocalcin; O-hDPSCs = osteogenic induced human dental pulp stem cells; *RunX2* = Runt-related transcription factor-2.

Runt-related transcription factor-2 (*RunX2*; 176bp) is essential for osteoblastic differentiation and according to RT-PCR results it is present in all samples, including control samples (Figure 16). Bands resulting from labeled and unlabeled control samples (1C,1S) are clearly less discernible compared to the band resulting from SPIO-labeled O-hDPSCs. However, when band intensities were normalized to the expression of *ActB* of the corresponding sample, only a minor difference remains (Figure 16C). For some cultures the difference between undifferentiated (2C,2S) and differentiated samples (2O⁻, 2O⁺) is more pronounced, even after normalization (Figure 16C). For both patients the *RunX2* expression in labeled (1S, 2S) and unlabeled (1C,2C) hDPSCs is very similar. Although differences in

RunX2 expression are seen between labeled (20^+) and unlabeled (20^-) O-hDPSCs, this variation is less pronounced than the difference between O-hDPSCs and undifferentiated control samples (2C,2S).

3.5.4 Osteogenic differentiation leads to an upregulation of the protein osteocalcin

In order to evaluate the osteoblastic phenotype, O-hDPSCs were subjected to immunocytochemical stainings with an antibody directed against the bone-specific protein osteocalcin (OCN). Control samples containing non-differentiated SPIO-labeled hDPSCs were found positive for OCN (Figure 17A). However, quantification of the mean fluorescent intensity yielded a significant ($p < 0.001$) increase in OCN reactivity in differentiated samples compared to control samples (Figure 17D). Based on measurements of the mean fluorescent intensities, no significant difference between labeled and unlabeled O-hDPSCs could be stated (Figure 17D). Negative control samples did not exhibit non-specific binding of secondary antibody (data not shown).

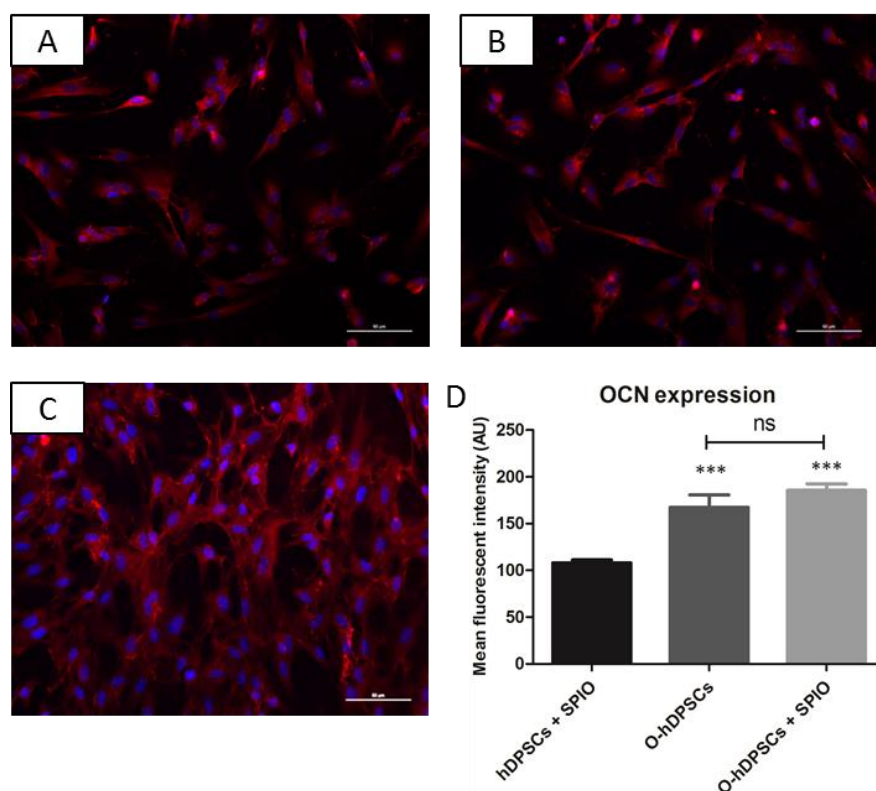


Figure 17: Osteogenic induced hDPSCs show significantly more immunoreactivity for OCN. After three weeks of osteogenic induction unlabeled (B) and SPIO-labeled O-hDPSCs (C) were stained with an antibody directed against OCN, to evaluate the acquired osteoblastic phenotype. The OCN expression was compared to the control conditions containing undifferentiated labeled hDPSCs (A). Both O-hDPSCs samples show immunoreactivity for OCN but undifferentiated labeled hDPSCs were also found to express OCN at protein level (A). Quantification of fluorescent intensity yielded a significant ($p < 0.001$) increase in immunoreactivity for OCN in labeled and unlabeled O-hDPSCs, compared to control samples. Furthermore, no significant difference between OCN immunoreactivity of labeled and unlabeled O-hDPSCs could be stated (D). Data were analyzed with One Way ANOVA and Tukeys multiple comparison post-test. Data are represented as S.E.M.; *** = p -value ≤ 0.001 . O-hDPSCs = osteogenic-induced human dental pulp stem cells; OCN = osteocalcin; SPIO = superparamagnetic iron oxide (Scale bar = $50\mu\text{m}$.)

3.5.5 T2* signal intensity is significantly decreased by 500 SPIO-labeled O-hDPSCs/ μL

In order to evaluate the possibility for long-term labeling, hDPSCs were labeled with 15 $\mu\text{g}/\text{mL}$ SPIO and 0.75 $\mu\text{g}/\text{mL}$ PLL prior to osteogenic differentiation. After three weeks of *in vitro* culturing O-hDPSCs were collected for phantom construction (n=2). 3D-T2*-weighted MR-images of the constructed phantoms show almost no perceptible increase in contrast with increasing concentrations of labeled O-hDPSCs (Figure 18A). The MRI scans were translated to relative T2* signal intensities and data were normalized by defining the control condition containing one labeled cell/ μL as 100% relative signal intensity (Figure 18B). The loading condition of 500 labeled O-hDPSCs results in a significant ($p < 0.01$) decrease in relative T2* signal intensity (Figure 18B).

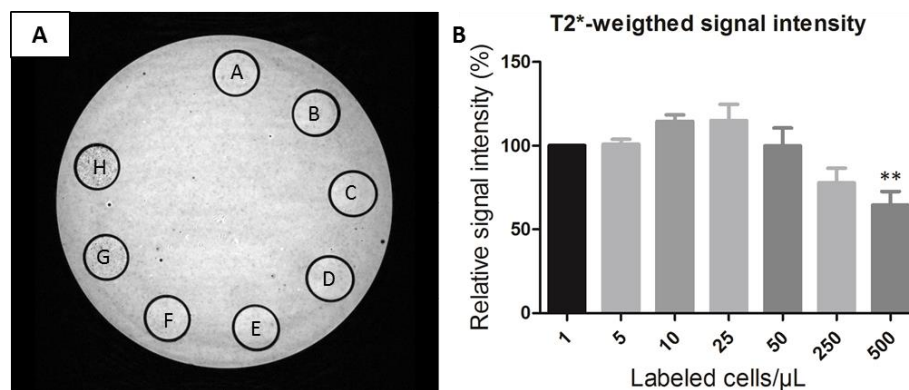


Figure 18: T2* signal intensity is significantly decreased by 500 SPIO-labeled O-hDPSCs/ μL . 3D- T2*-weighted MR-images of O-hDPSCs, three weeks after labeling with 15 $\mu\text{g}/\text{mL}$ SPIO and 0.75 $\mu\text{g}/\text{mL}$ PLL show almost no perceptible increase in MRI contrast (A). However, analysis of relative T2*-signal intensities demonstrate the ability of 500 SPIO-labeled O-hDPSCs/ μL to significantly ($p < 0.01$) decrease T2* signal intensities (B). Data were analyzed with one way ANOVA and Dunnett's multiple comparison post-test. Data are represented as S.E.M.; ** = p -value ≤ 0.01 . (A = 500 unlabeled cells/ μL ; B-C-D-E-F-G-H = respectively 1, 5, 10, 25, 50, 250 and 500 labeled cell(s)/ μL). O-hDPSCs = osteogenic induced human dental pulp stem cells; SPIO = superparamagnetic iron oxide; PLL = poly-L-lysine; MRI = magnetic resonance imaging.

3.5.6 Increasing SPIO concentrations leads to an increased accumulation of intracellular iron deposits

In order to increase detectability of labeled O-hDPSCs after three weeks of *in vitro* culture, hDPSCs were labeled with either 25 or 50 $\mu\text{g}/\text{mL}$ SPIO particles. Perls' staining indicated that increasing the SPIO concentrations was not associated with aberrations in cellular morphology (Figure 19A,C). Even with the increased amount of intracellular iron deposits, the labels remain mainly located within the peri-nuclear region (Figure 19A,C). However, labeling with 50 $\mu\text{g}/\text{mL}$ SPIO particles was associated with the presence of extracellular iron deposits, after 24 hours of label-free culture (Figure 19C, arrowhead). There was no evidence of extracellular iron deposits after labeling with 25 $\mu\text{g}/\text{mL}$ SPIO particles (Figure 19A). After three weeks of osteogenic induction, Perls' iron staining showed severe label dilution, with the presence of unlabeled cells in both labeling conditions (Figure 19B). However, samples labeled with 50 $\mu\text{g}/\text{mL}$ SPIO prior to osteogenic induction, contained a smaller fraction of

unlabeled cells (Figure 19D). Moreover, after three weeks of label-free culture, there was no evidence extracellular iron deposits (Figure 19D).

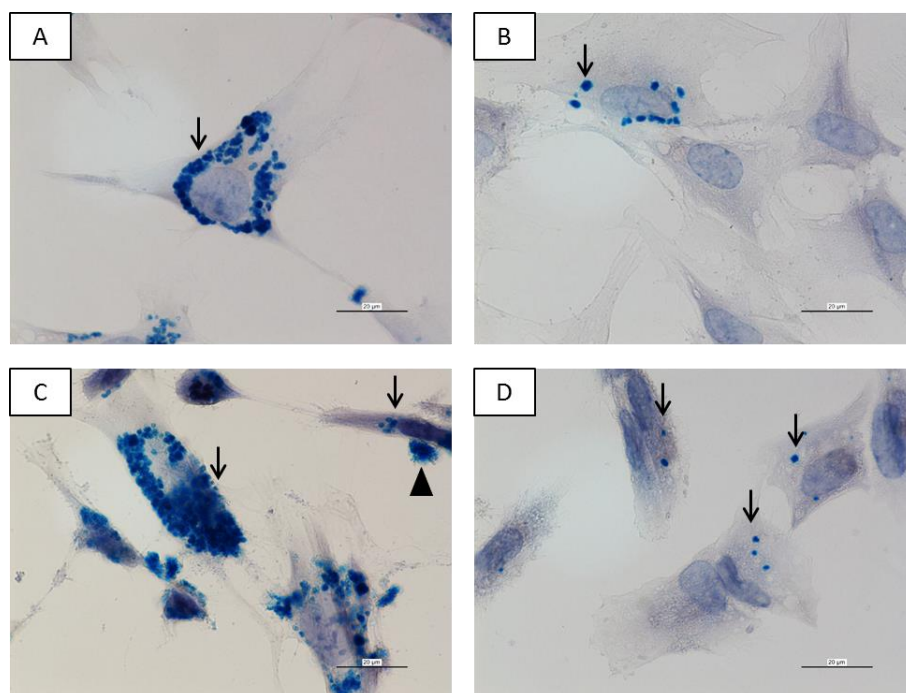


Figure 19: Increasing SPIO concentrations leads to an increased accumulation of intracellular iron deposits. Perl's iron staining shows intracellular iron deposits (arrows) 24 hours after labeling hDPSCs with 25 $\mu\text{g}/\text{mL}$ (A) or 50 $\mu\text{g}/\text{mL}$ (C) SPIO and 0.75 $\mu\text{g}/\text{mL}$ PLL. hDPSCs did not display morphological aberrations due to increased label content. However, labeling with 50 $\mu\text{g}/\text{mL}$ SPIO resulted in the presence of extracellular iron deposits (C, arrowhead) Despite the abundance of intracellular iron deposits, particles mainly reside within the peri-nuclear zone (A,C). After three weeks of osteogenic differentiation, SPIO concentrations were severely decreased and unlabeled cells were present in both O-hDPSCs cultures (B,D). However, labeling hDPSCs with 50 $\mu\text{g}/\text{mL}$ SPIO resulted in a smaller fraction of unlabeled cells after osteogenic induction (D). hDPSCs = human dental pulp stem cells; O-hDPSCs = osteogenic induced human dental pulp stem cells; PLL = poly-L-lysine; SPIO = superparamagnetic iron oxide (Scale bar =20 μm)

4 Discussion

Recent studies have identified hDPSCs as a promising cell type for future clinical applications [15]. Prior to clinical implementations, extensive pre-clinical research is necessary to clearly define cellular characteristics and ensure patient safety. Furthermore, tracking the migration of transplanted SCs *in vivo* is necessary to evaluate and improve stem cell therapy [34]. The aim of this study was twofold: firstly, this study investigated the effect of iron oxide labeling on the differentiation potential of hDPSCs. Therefore, hDPSCs were isolated from third molars and subjected to SPIO labeling prior to adipogenic and osteogenic differentiation. Secondly, the long-term label efficiency was evaluated by means of MR-imaging.

In this study hDPSCs were isolated from human impacted third molars via the explant methodology. When Gronthos *et al.* first described this stem cell population, hDPSCs were brought into culture using enzymatic digestion [12]. However, hDPSCs cultured via the explant methodology have been described to show increased proliferation and enhanced differentiation potential, compared to hDPSCs derived from enzymatic digestion [39]. Furthermore, according to Kerkis *et al.* the explant method results in a more homogeneous population of hDPSCs [40, 41]. For these reasons, the hDPSCs used in this study were derived from explant cultures.

In first instance, the MSC phenotype of the acquired hDPSCs populations was determined using the minimal criteria proposed by the International Society for Cellular Therapy. The first requirement of plastic adherence under standard culturing conditions was achieved in explant cultures of all patients included in this study. Secondly, in order to qualify as MSCs, the cell population must express certain MSC markers (CD105, CD146, CD90,..), while being negative for other markers (CD45, CD34, CD14 or CD11b, CD79 α or CD19). Prior to this study, our lab has published detailed data on the immunophenotype of hDPSCs cultured via the explant methodology [41]. In the present study CD105, CD146 and STRO-1 were selected from this list to check for the mesenchymal nature of the obtained cell cultures. The immunophenotype of the acquired hDPSCs populations was determined using immunocytochemistry. Immunocytochemical analysis demonstrated the expression of CD105 and CD146. Furthermore, the resulting hDPSCs populations also showed immunoreactivity for STRO-1, which is considered to be a marker for more potent MSCs [42]. Since discriminating MSCs from HSCs is mainly an issue when working with bone-marrow derived cultures, the absence of CD34 expression was not determined in current experiments. Finally, the resulting population should be capable of multi-lineage differentiation. The chondrogenic, adipogenic and osteogenic differentiation potential of explant-derived hDPSCs was already confirmed in previous research performed by our

lab [9]. Chondrogenic induction resulted in the production of glycosaminoglycans and glycoproteins and the expression of aggrecan, while adipogenic induced hDPSCs were described to contain lipid droplets and express FABP-4. Furthermore, Osteogenic differentiation resulted in the production of cross-banded collagen fibrils en *de novo* expression of osteocalcin [9].

One of the major goals of cell-based therapy is to transplant SCs to modulate the microenvironment and to achieve tissue replacement. Therefore, the SCs should be able to home and engraft into target tissues [19]. In order to closely monitor this process, SCs can be tagged with various techniques prior to transplantation. This study opted for the magnetic labeling of hDPSCs for several reasons. Firstly, magnetic labeling circumvents the need to genetically modify the SCs prior to transplantation, thereby limiting the risks of malignant transformation. Furthermore, clinically approved SPIO particles, such as Endorem[®] have been shown to be biodegradable [43]. Finally, the use of magnetic labels allows non-invasive *in vivo* tracking of the stem cells by means of MR-imaging, which is currently regarded as the most promising imaging strategy mainly due to its perfect soft tissue contrast [1, 34].

The present study investigated the effect of SPIO labeling on the differentiation capacity of hDPSCs. The working concentration of 15 $\mu\text{g}/\text{mL}$ SPIO conjugated to 0.75 $\mu\text{g}/\mu\text{L}$ PLL was based on previous research performed at our lab [22]. In accordance with previous reports from our lab, 24 hours labeling of hDPSCs with SPIO/PLL mixtures did not influence cell morphology as indicated by phase-contrast images. Twenty-four hours exposure to SPIO labels resulted in cellular uptake of SPIO particles as evidenced by the presence of blue precipitates after Perls' iron staining. Ultrastructural analysis confirmed the lack of morphological aberrations and showed the homogeneous distribution of SPIO particles within endosomes. Labeled hDPSCs were not subjected to more elaborate cell viability tests since several other studies (inclusive the study performed in our lab) reported no deleterious effects on cell viability [22, 44, 45].

SCs can be transplanted in order to modulate the microenvironment either immunologically or by secreting trophic factors [18, 46]. But when SCs are transplanted with the aim of tissue regeneration, they are expected to differentiate *in vivo* in order to replace damaged tissue. To replicate this process *in vitro*, hDPSCs in this study were subjected to *in vitro* differentiation towards adipogenic and osteogenic lineages prior to transplantation. Besides investigating the effect of SPIO labeling on adipogenic and osteogenic differentiation, this study also assessed long-term label retention. Demonstrating long-term label retention is important, since it will allow the close monitoring of transplanted SCs and thereby improving cell-based therapies.

Adipogenic induction of labeled hDPSCs with hydrocortisone, isobutylmethylxanthine and indomethacin resulted in similar morphological and ultrastructural changes as previously reported by our group for unlabeled hDPSCs [9]. In the case of SPIO labeled hDPSCs, adipogenic induction also lead to a more cuboidal morphology. Ultrastructural analysis demonstrated the presence of electron-dense intracellular lipid droplets as well as iron oxide-filled endosomes. Oil red O staining also confirmed that SPIO labeling did not inhibit the formation of lipid droplets in A-hDPSCs as evidenced by the co-localization of lipid droplets and SPIO particles. However not all cultured cells developed lipid droplets, which are characteristic for adipogenic differentiation. Adipogenic differentiation was also confirmed by the presence of cells showing strong immunoreactivity for FABP-4. Similar to the Oil red O staining, only a subset of cells was positive for FABP-4. Since a baseline expression was also detected in undifferentiated control samples, the limited amount of FABP-4 positive cells were not able to significantly alter the mean fluorescent intensity of differentiated samples. The yield of the differentiation process could possibly be increased by purifying the hDPSCs population, based on the expression of MSC surface markers.

Furthermore, adipogenic induction was also evaluated based on the expression of adipocyte specific makers at mRNA level as well as at protein level. At mRNA level, the expression of *LPL* was only detected in A-hDPSCs samples. These results are in agreement with RT-PCR data reported by Gronthos *et al.* [15]. Furthermore, *LPL* expression in labeled A-hDPSCs was equivalent to the expression level in unlabeled A-hDPSCs. In contrast to *LPL*, *PPAR- γ* was not only detected in differentiated cells but also in labeled and unlabeled control samples. Although Gronthos *et al.* reported a clear upregulation of *PPAR- γ* expression in A-hDPSCs, they also detected *PPAR- γ* expression in non-induced samples [15]. However, Um and colleagues reported the absence of *PPAR- γ* expression in non-induced samples [47]. Although *PPAR- γ* was found to be expressed in both hDPSCs and A-hDPSCs, analysis of band intensities and normalization to *ActB*, revealed a minor increase in *PPAR- γ* in differentiated samples. The normalized band intensity of A-hDPSCs was always higher compared to control samples, except for one cDNA sample of unlabeled A-hDPSCs. This outlier could be a consequence of variations in sample loading, therefore RT-PCR experiments should be repeated in order to acquire a more consistent dataset. The increase in *PPAR- γ* expression was most pronounced in the pure cDNA samples and the 1:2 dilution. Only one sample of unlabeled A-hDPSCs was included in this experiment due to insufficient RNA yield of the second sample. *PPAR γ* is an important transcription factor during early adipogenesis, while *LPL* is a mature marker of adipogenic differentiation, possibly explaining why only *LPL* expression was found to be restricted to A-hDPSCs [48-50]. Another explanation could also involve the insufficient specificity of the used primer pair for the adipocyte specific isoform *PPAR γ -2*, which is the isoform of *PPAR γ* predominantly expressed in

adipose tissue [50]. These results could be further elucidated by including more patient samples, by testing other primer pairs or by switching to more quantitative methods such as real-time PCR experiments. Taken together, these results indicate that labeling hDPSCs with 15 $\mu\text{g}/\text{mL}$ SPIO and 0.75 $\mu\text{g}/\text{mL}$ PLL does not interfere with their capacity for adipogenic differentiation.

Prior to adipogenic induction, hDPSCs were labeled for 24 hours and re-seeded in label-free medium for differentiation experiments. After three weeks of adipogenic induction, SPIO labels were detected with Perls' iron staining. A-hDPSCs were harvested for MRI-phantom construction. Increasing concentrations of labeled cells resulted in a gradual increase in MRI contrast on T2*-maps. When relative signal intensities were calculated a decreasing trend could be seen, starting at a concentration of 25 labeled cells/ μL . However, the concentration had to be further increased to 250 labeled A-hDPSCs/ μL in order to significantly decrease T2* signal intensity. Further incrementing cell density to 500 labeled A-hDPSCs/ μL did not cause a more pronounced decrease in T2* signal intensity. Although these results are in agreement with MRI-data from previous research, using identical labeling conditions, it is worth noting that Struys *et al.* already harvested labeled cells one and three days post-labeling [22]. Whereas, hDPSCs in this study were subjected to three weeks of label-free culture prior MRI-analysis. The relative high label content after three weeks of adipogenic induction can be explained by the fact that hDPSCs stop proliferating when transferred to adipogenic-inductive medium. These results from the *in vitro* MR-images indicate that labeling hDPSCs with 15 $\mu\text{g}/\text{mL}$ SPIO and 0.75 $\mu\text{g}/\text{mL}$ PLL is sufficient for cellular imaging after three weeks of adipogenic differentiation. Since further incrementing the number of labeled cells beyond 250 cells/ μL did not cause a more pronounced decrease in T2* signal intensity, this condition was used for *in vivo* experiments to monitor the long-term cell fate of labeled A-hDPSCs.

Transplanting 250 labeled A-hDPSCs/ μL into C57BL/6 mice completely diminished T2* relaxation. This concentration resulted in a ghosting artifact, leading to the loss of anatomical information of surrounding tissues, suggesting that a concentration of 250 labeled A-hDPSCs/ μL is too high for *in vivo* MR-imaging. The contradiction between the results of *in vitro* and *in vivo* T2*-weighted MR-images can be explained by the fact that in an *in vitro* setting, labeled cells are confined to a preset area and are homogeneously distributed. The use of agar as a loading vehicle in the *in vitro* studies implies total cell death of the loaded specimens. In contrast, *in vivo* transplantation was performed using Matrigel as a vehicle which in turn allows cell survival and migration. Therefore, possible *in vivo* cell clustering might therefore cause such ghosting artifacts. Future experiments should therefore be performed with lower concentrations of labeled A-hDPSCs or only label a particular subset of the used transplants.

In contrast to the T2*-weighted images, T2 relaxation time was not completely diminished by the presence of 250 labeled A-hDPSCs/ μL . The less pronounced effect of labeled A-hDPSCs on T2 relaxation compared to T2* relaxation can be explained by the fact that T2*-imaging is more susceptible for the field inhomogeneities caused by SPIO labeling than T2-imaging [27]. Analysis showed a significant decrease in T2 relaxation compared to unlabeled hDPSCs. Compared to other reports, this study acquired a significant decrease in T2 relaxation with a relative low SPIO concentration and a low amount of transplanted SCs [29, 31, 44, 51]. The current study only included MR-images 24 hours after Matrigel injection. However, animals will continue to be monitored until four weeks post injection in order to determine long-term *in vivo* label retention. MRI data will be used to monitor cell proliferation, since the resulting label dilution can be detected with MRI. Furthermore, if Matrigel plugs are still intact after a four week follow up period, they will be recovered for histological validation of the acquired MRI data. In order to exclude the possibility of SPIO leakage creating non-specific MRI signals, Perls' iron staining will be performed. Furthermore the differentiation stage of the A-hDPSCs will be evaluated based on Oil red O staining to demonstrate the presence of lipid droplets. Control hDPSCs will be monitored for possible dentin production. Gronthos *et al* reported dentin production of subcutaneously transplanted hDPSCs. However, Gronthos and colleagues used a mixture of 4×10^6 hDPSCs and hydroxyapatite/tricalcium ceramic powder as a transplant vehicle, while this study used growth factor-reduced Matrigel loaded with a total of 62500 hDPSCs. [15].

Osteogenic induction of SPIO-labeled hDPSCs with dexamethasone, ascorbatphosphate and β -glycerolphosphate, resulted in a multilayered cell population producing small calcified nodules, similar to other reports of unlabeled hDPSCs [9, 52, 53]. In contrast to the A-hDPSCs, O-hDPSCs underwent substantial label dilution during the *in vitro* culturing period. The considerable decrease in label content can be contributed to persistent cellular proliferation during osteogenic differentiation, which causes the endocytosed SPIO particles to be divided between proliferating cells. Successful osteogenic induction of labeled hDPSCs was confirmed by ultrastructural analysis, which demonstrated the capacity of SPIO-containing O-hDPSCs, to produce extracellular matrix, mainly consisting of cross-banded collagen fibrils.

Osteogenic induction was also evaluated based on gene expression of osteoblast-specific genes. *RunX2* gene expression was used to evaluate osteogenic induction, since it has been described as a master regulator of osteoblast development and bone formation [54]. *RunX2* was found to be expressed in both control samples as well as in labeled and unlabeled O-hDPSCs. In one patient the expression of *RunX2* seemed markedly more pronounced in the labeled O-hDPSC samples, however, after normalizing only a minor increase in optical density (OD) values could be demonstrated.

However, some patient samples showed a more pronounced increase in *RunX2* expression in differentiated samples. In these samples the variation between unlabeled and labeled O-hDPSCs was considerably less than the difference between undifferentiated and differentiated hDPSCs. All samples evaluated, displayed very similar expression levels of *RunX2* in labeled and unlabeled control samples, suggesting that SPIO labeling does not alter baseline *RunX2* expression levels. The presence of *RunX2* in undifferentiated hDPSCs is supported by data published by Karaöz *et al.* [55]. Furthermore *RunX2* has been described to be a specific transcription factor expressed in both mature osteoblasts and in MSCs. *RunX2* could mediate the differentiation from the pluripotent MSCs towards pre-osteoblasts and immature osteoblasts [56, 57].

Osteocalcin is considered a bone-specific protein and *osteocalcin* gene expression was used for the validation of osteogenic induction [58]. *Osteocalcin* was found to be expressed in both undifferentiated and differentiated samples. Analysis of band intensities and normalization to *ActB* revealed a minor increase in *OCN* expression in some samples of labeled and unlabeled O-hDPSCs. The apparent decrease in *OCN* expression in labeled O-hDPSCs from one patient is probably due to low expression of *ActB* in the labeled and unlabeled control samples. However, these samples did not display similar deviations when used for RT-PCR experiments relating to *PPAR-γ* expression, suggesting that the annealing temperature used for *OCN* and *RunX2* PCR reactions, might not be suitable for these particular samples. The annealing temperature of the *PPAR-γ* primer pair corresponds more closely to the annealing temperature of *ActB* primers. For future experiments, other, preferable more stable, housekeeping gene should be used. For both patients the OD values of labeled and unlabeled control samples are very similar, suggesting no changes in *OCN* expression were induced by the presence of SPIO particles. Our results which demonstrate *OCN* expression in undifferentiated hDPSCs are supported by previous reports by Mori *et al.* and Karbanova *et al.* [52, 53]. Because hDPSCs reside in a hard tissue environment, in close proximity to bone and dentin producing cells, the presence of *OCN* in native hDPSCs is not to peculiar. However, Li and colleagues only detected *OCN* expression after 21 days of osteogenic induction [59].

The expression of *OCN* on a protein level was also investigated using immunocytochemical analysis. Analogous to RT-PCR experiments, *OCN* protein expression was also detected in control samples. However quantification of fluorescent intensities yielded a significant increase in immunoreactivity for *OCN* in both labeled and unlabeled O-hDPSCs. The increased protein expression of *OCN* could lead to a depletion of *OCN* mRNA, thereby accounting for the only minor increase in *OCN* expression, detected by RT-PCR. Moreover, these results also support the previous suggestion that SPIO labeling does not interfere with the differentiation potential of hDPSCs, since no significant difference could be demonstrated between labeled and unlabeled O-hDPSCs.

hDPSCs were labeled with SPIO/PLL mixtures prior to osteogenic differentiation process. Perls' iron staining revealed a remarkable decrease in label content after osteogenic induction. The substantial label dilution is due to the continued proliferation of hDPSCs during osteogenic induction. During cell divisions, the content of the cytoplasm is distributed equally between the two daughter cells, thereby diluting the label content with every division. While increasing amounts of labeled A-hDPSCs result in a gradual increase in MRI contrast when detected by eye, 3D-T2* images reveal almost no detectable increase in contrast with increasing concentration of labeled O-hDPSCs. However, analysis of T2* values showed a significant decrease in T2* signal intensity could be obtained with 500 labeled O-hDPSCs/ μ L. In contrast to the A-hDPSCs, where 250 labeled cells/ μ L caused the T2* signal intensity to drop below 25% of the control condition, 500 labeled O-hDPSCs/ μ L only decreased the T2* signal intensity to about 60% of the control condition. However, this reduction did not sufficiently increase the detectability of the cells during visual interpretation of the MR-images. For this purpose, osteogenic differentiation was repeated with hDPSCs labeled with 25 μ g/mL SPIO particles prior to osteogenic differentiation.

Increasing SPIO concentrations to 25 and 50 μ g/mL resulted in an increase in intracellular iron deposits and did not affect hDPSCs morphology. Extracellular iron deposits were only detected after labeling with 50 μ g/mL, which is in accordance with previous reports from our lab [22]. Once transplanted, the presence of extracellular iron deposits may lead to non-specific MR signals due to SPIO transfer to host cells. However, the three weeks of label free culture, removed all extracellular iron deposits from the cultures, thereby eliminating the threat of non-specific SPIO uptake by host cells. However, it is still possible for *in vivo* cell death to cause SPIO leakage, resulting in non-specific SPIO transfer and consequently non-specific MR signals. Therefore, histological validation remains necessary to validate the specificity of the hypo-intense MR signals. Furthermore, our lab also reported no detrimental effects of these labeling conditions on short term cell viability [22]. Again, osteogenic differentiation lead to substantial label dilution with the presence of unlabeled cells. However, labeling with 50 μ g/mL resulted in the smallest fraction of unlabeled cells. In order to investigate whether the increase in SPIO concentration was sufficient to increase the detectability of the cells during visual interpretation of the MR-images, *in vitro* MR-imaging needs to be performed. After determination of optimal label conditions, *in vivo* experiments can be performed, analogous to the *in vivo* experiments performed with A-hDPSCs.

5 Conclusion & Synthesis

Cell therapy is an emerging area of research in the field of tissue regeneration and it is becoming a realistic alternative to conventional treatment options. Since the use of totipotent embryonic SCs is impeded by ethical considerations and risk of teratoma formation, (bio)medical research has shifted its focus onto easily accessible adult SCs. Recent studies have suggested hDPSCs to be suitable candidates for developing cell-based therapies. These adult MSCs display similar characteristics as bone-marrow derived MSCs, with the advantage that hDPSCs do not require invasive isolation procedures, since they can be harvested from surgical waste material. In order to guarantee safety and efficacy, SC-transplants need to be closely monitored. In this regard, magnetic resonance imaging has been suggested as an attractive image modality for *in vivo* stem cell tracking. Labeling the SCs with superparamagnetic iron oxide (SPIO) particles prior to transplantation, allows *in vivo* cell tracking using MR-imaging.

This study comprised two different parts, the first one being the evaluation of the adipogenic and osteogenic differentiation potential of SPIO-labeled hDPSCs. The adipogenic differentiation of SPIO-labeled hDPSCs was confirmed by histochemical and ultrastructural analysis, showing the presence of lipid droplets in labeled cells. However, only a subset of hDPSC acquired the adipocyte phenotype since not all cells produced lipid droplets and only a limited amount of FABP-4 positive cells were found in differentiated samples. In order to increase the yield of adipogenic differentiation, future experiments could opt for purification of the hDPSCs population based on the presence of MSC surface markers. Furthermore, RT-PCR experiments demonstrated *de novo* expression of LPL at mRNA level as well as a slight upregulation of PPAR- γ in some of the differentiated cultures. Osteogenic induction of SPIO-labeled hDPSCs resulted in the production of cross-banded collagen fibrils and calcified extracellular matrix as demonstrated by TEM analysis and an upregulation of osteocalcin at protein level. Similarly, RT-PCR confirmed the expression of OCN by non-differentiated cells, but at mRNA level, only a minor increase in expression levels could be demonstrated. Furthermore, RunX2 was also found to be expressed in both differentiated and undifferentiated hDPSCs, however, some samples displayed a more pronounced increase in *RunX2* expression in O-hDPSCs. Since none of the experiments resulted in significant, or otherwise obvious, differences between labeled and unlabeled O-hDPSCs, we conclude that SPIO labeling neither interferes with adipogenic nor with osteogenic differentiation of hDPSCs.

The second part of this study focused on the use of SPIO particles for long-term cell tracking. In this regard, hDPSCs were labeled with 15 $\mu\text{g}/\text{mL}$ SPIO combined with 0.75 $\mu\text{g}/\text{mL}$ PLL prior to adipogenic and osteogenic differentiation. After adipogenic induction, hDPSCs (250 cells/ μL) contained sufficient SPIO particles to significantly decrease T2* signal intensities, thereby demonstrating sufficient label retention under these particular experimental conditions. To further elucidate the possibilities of SPIO labeling for *in vivo* cell tracking, hDPSCs and labeled A-hDPSCs were transplanted into C57BL/6 mice. Inhomogeneous distribution of labeled A-hDPSCs within the Matrigel lead to complete T2* signal quenching. Due to this ghosting artifact, anatomical information was lost on T2*-weighted MR-images. Analysis of T2-weighted MR-images revealed a significant decrease in T2 relaxation time in the presence of 250 labeled A-hDPSCs/ μL , without completely quenching the T2 signal. A higher concentration of O-hDPSCs (500cells/ μL) was necessary to significantly decrease T2* signal intensities and the changes in MRI contrast were less distinct compared to the contrast-changes seen with A-hDPSCs. In order to address this problem, the SPIO concentration was increased to 25 and 50 $\mu\text{g}/\text{mL}$ prior to osteogenic induction. Similar to the previous labeling condition with 15 $\mu\text{g}/\text{mL}$ SPIO, Perl's iron staining revealed a substantial label dilution, with the lowest amount of unlabeled cells in the cultures labeled with 50 $\mu\text{g}/\text{mL}$. Therefore, future MRI phantoms are to determine whether labeling with 25 $\mu\text{g}/\text{mL}$ SPIO was sufficient to increase the detectability of O-hDPSCs during visual interpretation of the MR images or if this can only be achieved by labeling with 50 $\mu\text{g}/\text{mL}$ SPIO particles.

In conclusion, this study provides evidence that SPIO labeling does not interfere with the adipogenic and osteogenic differentiation potential of hDPSCs. SPIO labeling was not found to alter the expression of lineage specific markers or interfere with either lipid or collagen production. Furthermore, we demonstrated that labeling conditions need to be optimized for each experimental setup. While labeling with 15 $\mu\text{g}/\text{mL}$ SPIO particles sufficiently altered MRI contrast, for the detection of A-hDPSCs during visual interpretation of MR-images, this was not the case for O-hDPSCs. Finally, *in vivo* MRI data provide promising results for the non-invasive monitoring of SPIO-labeled A-hDPSCs.

6 References

1. Himmelreich, U. and T. Dresselaers, *Cell labeling and tracking for experimental models using magnetic resonance imaging*. Methods, 2009. **48**(2): p. 112-24.
2. Prockop, D.J., et al., *Defining the risks of mesenchymal stromal cell therapy*. Cytotherapy, 2010. **12**(5): p. 576-8.
3. Till, J.E. and C.E. Mc, *A direct measurement of the radiation sensitivity of normal mouse bone marrow cells*. Radiat Res, 1961. **14**: p. 213-22.
4. Gurudutta, G.U., et al., *Stem cell therapy: a novel & futuristic treatment modality for disaster injuries*. Indian J Med Res, 2012. **135**: p. 15-25.
5. Tirino, V., et al., *Methods for the identification, characterization and banking of human DPSCs: current strategies and perspectives*. Stem Cell Rev, 2011. **7**(3): p. 608-15.
6. Dominici, M., et al., *Minimal criteria for defining multipotent mesenchymal stromal cells. The International Society for Cellular Therapy position statement*. Cytotherapy, 2006. **8**(4): p. 315-7.
7. Le Blanc, K., et al., *HLA expression and immunologic properties of differentiated and undifferentiated mesenchymal stem cells*. Exp Hematol, 2003. **31**(10): p. 890-6.
8. Caplan, A.I., *Adult mesenchymal stem cells for tissue engineering versus regenerative medicine*. J Cell Physiol, 2007. **213**(2): p. 341-7.
9. Struys, T., et al., *Ultrastructural and immunocytochemical analysis of multilineage differentiated human dental pulp- and umbilical cord-derived mesenchymal stem cells*. Cells Tissues Organs, 2011. **193**(6): p. 366-78.
10. Erices, A., P. Conget, and J.J. Minguell, *Mesenchymal progenitor cells in human umbilical cord blood*. Br J Haematol, 2000. **109**(1): p. 235-42.
11. Zuk, P.A., et al., *Human adipose tissue is a source of multipotent stem cells*. Mol Biol Cell, 2002. **13**(12): p. 4279-95.
12. Gronthos, S., et al., *Postnatal human dental pulp stem cells (DPSCs) in vitro and in vivo*. Proc Natl Acad Sci U S A, 2000. **97**(25): p. 13625-30.
13. Shi, S., et al., *The efficacy of mesenchymal stem cells to regenerate and repair dental structures*. Orthod Craniofac Res, 2005. **8**(3): p. 191-9.
14. Volponi, A.A., Y. Pang, and P.T. Sharpe, *Stem cell-based biological tooth repair and regeneration*. Trends Cell Biol, 2010. **20**(12): p. 715-22.
15. Gronthos, S., et al., *Stem cell properties of human dental pulp stem cells*. J Dent Res, 2002. **81**(8): p. 531-5.
16. Huang, G.T., S. Gronthos, and S. Shi, *Mesenchymal stem cells derived from dental tissues vs. those from other sources: their biology and role in regenerative medicine*. J Dent Res, 2009. **88**(9): p. 792-806.
17. Kiraly, M., et al., *Integration of neuronally predifferentiated human dental pulp stem cells into rat brain in vivo*. Neurochem Int, 2011. **59**(3): p. 371-81.
18. Rasmusson, I., *Immune modulation by mesenchymal stem cells*. Exp Cell Res, 2006. **312**(12): p. 2169-79.
19. Kidd, S., et al., *Direct evidence of mesenchymal stem cell tropism for tumor and wounding microenvironments using in vivo bioluminescent imaging*. Stem Cells, 2009. **27**(10): p. 2614-23.
20. Sordi, V., *Mesenchymal stem cell homing capacity*. Transplantation, 2009. **87**(9 Suppl): p. S42-5.
21. Suzuki, T., et al., *Induced migration of dental pulp stem cells for in vivo pulp regeneration*. J Dent Res, 2011. **90**(8): p. 1013-8.
22. Struys, T., et al., *Magnetic resonance imaging of human dental pulp stem cells in vitro and in vivo*. Cell Transplant, 2012.

23. Weissleder, R., et al., *Magnetically labeled cells can be detected by MR imaging*. J Magn Reson Imaging, 1997. **7**(1): p. 258-63.
24. Bulte, J.W., et al., *Magnetodendrimers allow endosomal magnetic labeling and in vivo tracking of stem cells*. Nat Biotechnol, 2001. **19**(12): p. 1141-7.
25. Hendee, W.R. and C.J. Morgan, *Magnetic resonance imaging. Part I--physical principles*. West J Med, 1984. **141**(4): p. 491-500.
26. Brown, M.A. and R.C. Semelka, *MRI : basic principles and applications*. 3rd ed 2003, Hoboken, N.J.: Wiley-Liss. xiv, 265 p.
27. Chavhan, G.B., et al., *Principles, techniques, and applications of T2*-based MR imaging and its special applications*. Radiographics, 2009. **29**(5): p. 1433-49.
28. Aime, S., et al., *Insights into the use of paramagnetic Gd(III) complexes in MR-molecular imaging investigations*. J Magn Reson Imaging, 2002. **16**(4): p. 394-406.
29. Bulte, J.W. and D.L. Kraitchman, *Iron oxide MR contrast agents for molecular and cellular imaging*. NMR Biomed, 2004. **17**(7): p. 484-99.
30. Caravan, P., et al., *Gadolinium(III) Chelates as MRI Contrast Agents: Structure, Dynamics, and Applications*. Chem Rev, 1999. **99**(9): p. 2293-352.
31. Kustermann, E., et al., *Efficient stem cell labeling for MRI studies*. Contrast Media Mol Imaging, 2008. **3**(1): p. 27-37.
32. Andreas, K., et al., *Highly efficient magnetic stem cell labeling with citrate-coated superparamagnetic iron oxide nanoparticles for MRI tracking*. Biomaterials, 2012. **33**(18): p. 4515-25.
33. Wang, L., et al., *Superparamagnetic iron oxide does not affect the viability and function of adipose-derived stem cells, and superparamagnetic iron oxide-enhanced magnetic resonance imaging identifies viable cells*. Magn Reson Imaging, 2009. **27**(1): p. 108-19.
34. Zhang, H., *Iron oxide nanoparticles-poly-L-lysine complex*, in *Molecular Imaging and Contrast Agent Database (MICAD)2004*: Bethesda (MD).
35. Chen, Y.C., et al., *The inhibitory effect of superparamagnetic iron oxide nanoparticle (Ferucarbotran) on osteogenic differentiation and its signaling mechanism in human mesenchymal stem cells*. Toxicol Appl Pharmacol, 2010. **245**(2): p. 272-9.
36. Huang, D.M., et al., *The promotion of human mesenchymal stem cell proliferation by superparamagnetic iron oxide nanoparticles*. Biomaterials, 2009. **30**(22): p. 3645-51.
37. Soenen, S.J., et al., *Intracellular nanoparticle coating stability determines nanoparticle diagnostics efficacy and cell functionality*. Small, 2010. **6**(19): p. 2136-45.
38. Struys, T., et al., *Magnetic resonance imaging of human dental pulp stem cells in vitro and in vivo; Accepted in Cell Transplantation*.
39. Spath, L., et al., *Explant-derived human dental pulp stem cells enhance differentiation and proliferation potentials*. J Cell Mol Med, 2010. **14**(6B): p. 1635-44.
40. Kerkis, I. and A.I. Caplan, *Stem cells in dental pulp of deciduous teeth*. Tissue Eng Part B Rev, 2012. **18**(2): p. 129-38.
41. Hilkens, P., et al., *Effect of isolation methodology on stem cell properties and multilineage differentiation potential of human dental pulp stem cells*. Cell Tissue Res, 2013.
42. Yang, X., et al., *Multilineage potential of STRO-1+ rat dental pulp cells in vitro*. J Tissue Eng Regen Med, 2007. **1**(2): p. 128-35.
43. Weissleder, R., et al., *Superparamagnetic iron oxide: pharmacokinetics and toxicity*. AJR Am J Roentgenol, 1989. **152**(1): p. 167-73.
44. Soenen, S.J., A.R. Brisson, and M. De Cuyper, *Addressing the problem of cationic lipid-mediated toxicity: the magnetoliposome model*. Biomaterials, 2009. **30**(22): p. 3691-701.
45. Stroh, A., et al., *Iron oxide particles for molecular magnetic resonance imaging cause transient oxidative stress in rat macrophages*. Free Radic Biol Med, 2004. **36**(8): p. 976-84.
46. Jones, B.J. and S.J. McTaggart, *Immunosuppression by mesenchymal stromal cells: from culture to clinic*. Exp Hematol, 2008. **36**(6): p. 733-41.

47. Um, S., et al., *Effect of leptin on differentiation of human dental stem cells*. Oral Dis, 2011. **17**(7): p. 662-9.
48. Karagianni, M., et al., *A comparative analysis of the adipogenic potential in human mesenchymal stromal cells from cord blood and other sources*. Cytotherapy, 2013. **15**(1): p. 76-88.
49. Subash-Babu, P. and A.A. Alshatwi, *Aloe-emodin inhibits adipocyte differentiation and maturation during in vitro human mesenchymal stem cell adipogenesis*. J Biochem Mol Toxicol, 2012. **26**(8): p. 291-300.
50. Tontonoz, P., E. Hu, and B.M. Spiegelman, *Stimulation of adipogenesis in fibroblasts by PPAR gamma 2, a lipid-activated transcription factor*. Cell, 1994. **79**(7): p. 1147-56.
51. Crabbe, A., et al., *Effects of MRI contrast agents on the stem cell phenotype*. Cell Transplant, 2010. **19**(8): p. 919-36.
52. Karbanova, J., et al., *Characterization of dental pulp stem cells from impacted third molars cultured in low serum-containing medium*. Cells Tissues Organs, 2011. **193**(6): p. 344-65.
53. Mori, G., et al., *Dental pulp stem cells: osteogenic differentiation and gene expression*. Ann N Y Acad Sci, 2011. **1237**: p. 47-52.
54. Zanatta, M., et al., *Runx-2 gene expression is associated with age-related changes of bone mineral density in the healthy young-adult population*. J Bone Miner Metab, 2012. **30**(6): p. 706-14.
55. Karaoz, E., et al., *Human dental pulp stem cells demonstrate better neural and epithelial stem cell properties than bone marrow-derived mesenchymal stem cells*. Histochem Cell Biol, 2011. **136**(4): p. 455-73.
56. Morra, M., et al., *Gene expression of markers of osteogenic differentiation of human mesenchymal cells on collagen I-modified microrough titanium surfaces*. J Biomed Mater Res A, 2011. **96**(2): p. 449-55.
57. Marie, P.J., *Transcription factors controlling osteoblastogenesis*. Arch Biochem Biophys, 2008. **473**(2): p. 98-105.
58. Lee, N.K., et al., *Endocrine regulation of energy metabolism by the skeleton*. Cell, 2007. **130**(3): p. 456-69.
59. Li, J.H., et al., *Human dental pulp stem cell is a promising autologous seed cell for bone tissue engineering*. Chin Med J (Engl), 2011. **124**(23): p. 4022-8.
60. Nosrat, I.V., et al., *Dental pulp cells produce neurotrophic factors, interact with trigeminal neurons in vitro, and rescue motoneurons after spinal cord injury*. Dev Biol, 2001. **238**(1): p. 120-32.
61. Martens, W., et al., *Expression Pattern of Basal Markers in Human Dental Pulp Stem Cells and Tissue*. Cells Tissues Organs, 2012.
62. Sasaki, R., et al., *Neurosphere generation from dental pulp of adult rat incisor*. Eur J Neurosci, 2008. **27**(3): p. 538-48.
63. Arthur, A., et al., *Adult human dental pulp stem cells differentiate toward functionally active neurons under appropriate environmental cues*. Stem Cells, 2008. **26**(7): p. 1787-95.

Supplemental information

As mentioned, hDPSCs are multipotent cells, capable of differentiating into cells of odontogenic, adipogenic, osteogenic and chondrogenic lineages. However, due to their neural-crest origin, numerous studies have focused on the plasticity of hDPSCs to transdifferentiate towards neurogenic lineages. Furthermore, hDPSCs have been described to express neural markers and to produce and secrete neurotrophic factors [60, 61]. Moreover, hDPSCs have been reported to form neurospheres *in vitro* and differentiate into functionally active neurons [62, 63]. Taken together, all these characteristics make hDPSCs attractive candidates for cellular therapies for neurological disorders. The pilot study included in this study investigated whether neurogenic differentiation can be accomplished in SPIO-labeled hDPSCs.

S1. Supplemental materials & methods

S1.1 Neurogenic differentiation of hDPSCs

For neurogenic differentiation, culture flasks were coated with 10 µg/mL PLL for one hour at room temperature. Following trypsinisation, cells were kept in cell culture flasks (25cm²; Nunc, Denmark, Roskilde) at a density of 3 x 10⁴ cells/cm². Cells were kept in neurobasal medium (Invitrogen) supplemented with 1% P/S, 2% B27, 1% N2 supplement, 100 ng/mL bFGF, 20 ng/mL EGF, 10 ng/mL FGF-8 and 100 ng/mL SHH. Cells were cultured at 37°C in a humidified atmosphere containing 5% CO₂ and medium was changed every 3-4 days. After 6-8 days neurospheres were harvested and transferred to poly-L-ornithine (15 µg/ml; Sigma-Aldrich, Bornem, Belgium) and laminin (2 µg/ml; R&D systems, Minneapolis, MN, United States of America) coated glass-or Thermanox® coverslips. Mature neurospheres were kept in maturation medium consisting of neurobasal medium supplemented with 1 mM dbcAMP, 30 ng/mL NT-3, 2% B27 and 1% N2 supplement. Maturation medium was changed every 3-4 days. After 14 days, when cells had migrated out of the neurospheres to form a monolayer, they were fixed. Cells seeded on glass coverslips were washed with PBS and fixed with 4% formaldehyde for 20 min at room temperature. Cells seeded on plastic coverslips were fixed with 2% glutaraldehyde in 0.05M cacodylate buffer (pH 7.3) overnight at 4°C.

S2. Supplemental data

S2.1 SPIO labeling does not interfere with neurosphere formation or cellular outgrowth

hDPSCs were labeled with 15 µg/mL SPIO and 0.75 µg/mL PLL prior to starting the differentiation procedure. For the induction of neurogenic differentiation, labeled hDPSCs were seeded at a density of 30 000 cells/cm² onto PLL-coated culture flasks. Cultivating the hDPSCs in neurobasal medium

containing bFGF, EGF, FGF-8, SHH, B27 and N2 resulted in the formation of free floating neurospheres (Figure S1A-B). After only one day of neurogenic induction, cells already clustered and after four days of neurogenic induction, free floating neurospheres were present (Figure S1B). After seven days of neurogenic induction, neurospheres were harvested and transferred to poly-L-ornithin/laminin coated coverslips for the maturation phase. Neurospheres adhered to the coated-coverslips and cellular outgrowth was seen after one day of maturation (Figure S1C). After four days in culture, cells had died due to contamination of the NT-3 supplement and the experiment was discontinued (Figure S1D).

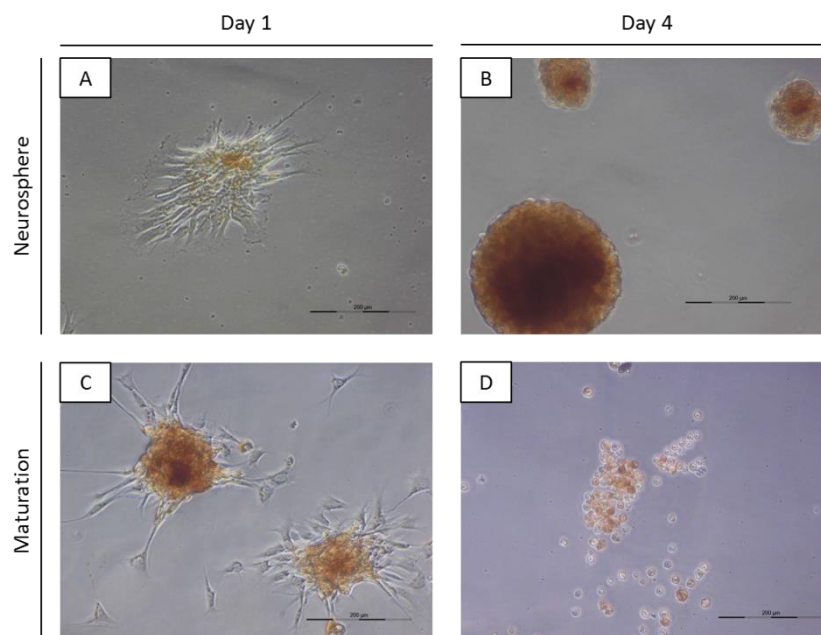


Figure S1: SPIO/PLL labeling of hDPSCs does not interfere with neurosphere formation and cellular outgrowth. Neurogenic induction lead to cellular clustering after one day of culture **(A)** and the formation of free floating neurospheres after four days of culture **(B)**. Transferring neurospheres to poly-L-ornithin/laminin coated coverslips and maturation medium, lead to the attachment of neurospheres and cellular outgrowth **(C)**. Four days into the maturation phase the experiment was discontinued due to contamination. hDPSCs= human dental pulp stem cells; PLL = poly-L-lysine; SPIO = superparamagnetic iron oxide (scale bar = 200µm)

Auteursrechtelijke overeenkomst

Ik/wij verlenen het wereldwijde auteursrecht voor de ingediende eindverhandeling:

Evaluation of iron oxide labeling as a tool for long term cell tracking and its effects on human dental pulp stem cell differentiation

Richting: **master in de biomedische wetenschappen-klinische en moleculaire wetenschappen**

Jaar: **2013**

in alle mogelijke mediaformaten, - bestaande en in de toekomst te ontwikkelen - , aan de Universiteit Hasselt.

Niet tegenstaand deze toekenning van het auteursrecht aan de Universiteit Hasselt behoud ik als auteur het recht om de eindverhandeling, - in zijn geheel of gedeeltelijk -, vrij te reproduceren, (her)publiceren of distribueren zonder de toelating te moeten verkrijgen van de Universiteit Hasselt.

Ik bevestig dat de eindverhandeling mijn origineel werk is, en dat ik het recht heb om de rechten te verlenen die in deze overeenkomst worden beschreven. Ik verklaar tevens dat de eindverhandeling, naar mijn weten, het auteursrecht van anderen niet overtreedt.

Ik verklaar tevens dat ik voor het materiaal in de eindverhandeling dat beschermd wordt door het auteursrecht, de nodige toelatingen heb verkregen zodat ik deze ook aan de Universiteit Hasselt kan overdragen en dat dit duidelijk in de tekst en inhoud van de eindverhandeling werd genotificeerd.

Universiteit Hasselt zal mij als auteur(s) van de eindverhandeling identificeren en zal geen wijzigingen aanbrengen aan de eindverhandeling, uitgezonderd deze toegelaten door deze overeenkomst.

Voor akkoord,

Ratajczak, Jessica

Datum: **10/06/2013**